NOVA SCHOOL OF SCIENCE & TECHNOLOGY

DEPARTMENT OF PHYSICS

MARGARIDA PATRÍCIO GOUVEIA

BSc in Biomedical Engineering

EVALUATION OF BRAIN VASCULARIZATION VIA FLOW ANALYSIS

AN ARTERIAL AND VENOUS HEMODYNAMIC STUDY WITH 4D PC-MRI

MASTER IN BIOMEDICAL ENGINEERING

NOVA University Lisbon
september, 2023

NOVA SCHOOL OF SCIENCE & TECHNOLOGY

DEPARTMENT OF PHYSICS

EVALUATION OF BRAIN VASCULARIZATION VIA FLOW ANALYSIS

AN ARTERIAL AND VENOUS HEMODYNAMIC STUDY WITH 4D PC-MRI

MARGARIDA PATRÍCIO GOUVEIA

BSc in Biomedical Engineering

Adviser: Ricardo Vigário
Associate Professor, NOVA University Lisbon

Co-adviser: Pedro Vilela
Neuroradiologist, Hospital da Luz

Examination Committee

Chair: Célia Maria Reis Henriques
Associate Professor, NOVA University Lisbon

Rapporteur: Patrícia Margarida Piedade Figueiredo
Associate Professor, University of Lisbon

Adviser: Ricardo Nuno Pereira Verga e Afonso Vigário
Associate Professor, NOVA University Lisbon

MASTER IN BIOMEDICAL ENGINEERING

NOVA University Lisbon
september, 2023

Evaluation of Brain Vascularization via Flow Analysis
An Arterial and Venous Hemodynamic Study with 4D PC-MRI

This document was created with the (pdf/Xe/Lua)LaTeX processor and the NOVAthesis template (v6.10.18) [1].

Acknowledgements

There are many remarkable people who shaped my academic journey and to all of them a want to express my gratitude.

First of all, I would like to express my deepest gratitude to my advisors, Professor Ricardo Vigário and Dr. Pedro Vilela, for providing me the opportunity to work on this thesis and for their guidance throughout the past months. I am grateful to Professor Ricardo for his support, words of encouragement, and belief in the success of this work. I would also like to extend my appreciation to Dr. Pedro for sharing his knowledge, dedication, and willingness to overcome every challenge that arose.

I am also very grateful for the opportunity to work at *Hospital da Luz* and have access to top-quality equipment, which was essential for the development of this thesis. I would like to thank technician Cristina for her collaboration in image acquisition, her help with data extraction, and dedication to this project.

I would also like to express my appreciation to Pablo Garcia-Polo for his constant availability and willingness to help, even from a different country. And a special thanks to Eng. Rogério for his assistance and support.

I would like to extend my gratitude to Eric Schrauben for developing the 4D Pulse Wave Velocity Tool and for addressing all my doubts and inquiries regarding its usage. I also want to express my heartfelt appreciation to Ana Duarte for all the advice, support, availability and for the incredible work she had previously undertaken, which laid a solid foundation for the development of this thesis.

I would also like to express my appreciation to all the volunteers who participated in this study. I am grateful for their contribution, and the enthusiasm they brought to each day of the study, as I heard from some of them, "It is satisfying to end the day with the feeling that I have made a contribution to science". To Miguel Lopes, with whom I shared both good and challenging days at *Hospital da Luz*, I'd like to thank for all the help during this project.

I would like to express my sincere gratitude to all my "friends from the university", the ones with whom I shared mornings in classes and mornings at the beach, evenings in the library and evenings at Tia's, nights of studying and nights of partying.

To all my friends from Tavira I would like to thank for making every 4 hour bus ride worth taking.

Lastly, but certainly not least, I want to express my deepest gratitude to all my XXL family. To my mom and dad, to my sisters, Matilde and Mafalda, to my brother, Hugo, to my niece and nephew, Artur and Carolina, and to Maryna. A heartfelt thank you for the support every step of the way and for always believing in me.

”

“Nanos gigantum humeris insidentes”

— Bernard of Chartres, 12th century
(Philosopher, scholar and administrator)

Abstract

Four-dimensional magnetic resonance angiography is a powerful tool for investigating the dynamics of blood flow in arteries, veins, and venous sinuses. When applied to the study of cerebral hemodynamics, this technique can play a crucial role in understanding and diagnosing various brain diseases and neurodegenerative disorders at an early stage.

To ensure the clinical applicability of this imaging technique, it is essential to validate its effectiveness. Therefore, the objective of this thesis work was, first and foremost, to study the reproducibility of measurements performed with this technique, namely the measurement of minimum, maximum, and average blood velocities, as well as the cross-sectional area of the internal carotid, middle cerebral, and basilar arteries. The measurements were conducted twice in 7 healthy individuals, between May and June.

The results of the reproducibility study were generally satisfactory, although the accuracy of measuring the cross-sectional area of the basilar artery and the middle cerebral artery was compromised. These inaccuracies were attributed to noise resulting from the high value for the velocity encoding employed.

Another objective of this thesis was to conduct a comprehensive study of the arterial and venous system in cerebral circulation. To achieve this, various parameters such as Pulsatility Index, Wall Stress, Pressure Drops, and Pulse Wave Velocity were calculated.

These parameters were compared with the existing data from the literature, and it was found that they were slightly overestimated. This overestimation was justified by the fact that these parameters are the result of calculations that use velocities, which were already overestimated themselves. The probable cause attributed to the overestimation of velocity was, once again, the high level of noise.

Keywords: Magnetic Resonance Angiography 4D, Hemodynamic Biomarkers, Cerebral Blood Flow, Brain Diseases, Cerebral Arteries, Venous Dural Sinuses

Resumo

A angiografia por ressonância magnética a quatro dimensões é uma ferramenta poderosa para o estudo da dinâmica do fluxo sanguíneo nas artérias, veias e seios venosos. Quando aplicada ao estudo da hemodinâmica cerebral, esta técnica pode desempenhar um papel importante na compreensão e diagnóstico precoce de várias doenças cerebrais.

Para que esta técnica de imagem possa ser utilizada na prática clínica, é necessário validar sua eficácia. Assim sendo, o objetivo deste trabalho de tese foi, em primeiro lugar, estudar a reprodutibilidade das medições realizadas com esta técnica, nomeadamente a medição das velocidades mínima, máxima e média do sangue e a área da secção transversal das artérias carótidas internas, cerebrais médias e basilar. As medições foram feitas em 7 indivíduos saudáveis, 2 vezes, entre maio e junho.

Os resultados deste estudo de reprodutibilidade foram satisfatórios, o parâmetro com pior resultado foi a área da secção transversal das artérias basilar e cerebral média. A explicação dada para os piores resultados deste estudo foi o alto nível de ruído, resultante do valor elevado da velocidade de codificação.

Outro objetivo deste trabalho foi realizar um estudo das artérias e veias cerebrais. Para isso, vários parâmetros foram calculados, como o Índice de Pulsatilidade, Stress na Parede Arterial, Quedas de Pressão e Velocidade da Onda de Pulso.

Os resultados deste estudo foram comparados com os valores já existentes na literatura e constatou-se que alguns parâmetros estavam um pouco sobrestimados. Esta sobrestimação, foi justificada por estes parâmetros serem resultado de cálculos que usam velocidades, estas que por si já estavam sobrestimadas. A provável causa atribuida à sobrestimação da velocidade foi, mais uma vez, o alto nível de ruído.

Palavras-chave: Ressonância Magnética de Fluxo 4D, Biomarcadores Hemodinâmicos, Fluxo Sanguíneo Cerebral, Doenças Cerebrais, Artérias Cerebrais, Seios Venosos Cerebrais

Contents

List of Figures

List of Tables

Abbreviations

2D Two-dimensional *(pp. 2, 8, 30)*
3D Three-dimensional *(pp. 2, 8)*
4D Four-dimensional *(pp. 2–4, 8–10, 13, 14, 19, 24, 30, 31)*

BA Basilar Artery *(pp. 4, 9, 14, 15, 17, 21–24, 26, 28–30, 32–34, 36, 37)*

C3 Cavernous Segment *(p. 14)*
CBF Cerebral Blood Flow *(pp. 1, 2, 4, 9–11)*
CI Confident Interval *(pp. 18, 20, 21)*
CNS Central Nervous System *(p. 1)*
CSVD Cerebral Small Vessels Disease *(pp. 1, 2, 4, 6, 7, 9–11, 39, 40)*
CT Computed Tomography *(p. 2)*

FVP Flow Volume Pulsatility *(pp. 2, 3, 7, 9–11, 15, 25, 33, 38)*

ICA Internal Carotid Artery *(pp. 4, 9–11, 14–17, 21–26, 28–34, 36)*
ICC Intraclass Correlation Coefficient *(pp. 18, 20, 21, 27–29)*
IJV Internal Jugular Vein *(pp. 5, 17, 18, 35, 36)*

LoA Limits of agreement *(pp. 18, 24, 29)*

M1 Sphenoidal Segment *(p. 14)*
MCA Middle Carotid Artery *(pp. 4, 9–11, 14, 15, 21, 22, 26, 28, 30, 32–34, 37)*
MD Mean Relative Difference *(pp. 18, 24)*
MRA Magnetic Resonance Angiography *(p. 7)*
MRI Magnetic Resonance Imaging *(pp. 1, 2, 7, 9, 12)*

PC-MRI Phase-Contrast Magnetic Resonance Imaging *(pp. 2–4, 7–10, 30)*
PD Pressure Drop *(pp. 2, 3, 7, 16, 17, 26, 35, 38)*

PI Pulsatility Index *(pp. 2, 3, 7, 9–11, 15, 25, 33, 38, 39)*
PWV Pulse Wave Velocity *(pp. 2, 3, 7, 16, 26, 34, 35, 38)*

r Pearson Correlation Coefficient *(pp. 18, 22, 28)*

SS Sigmoid Sinus *(pp. 17, 18)*
SSS Superior Sagittal Sinus *(pp. 5, 14, 24, 25, 31–33)*

TCD Transcranial Doppler *(pp. 9, 11, 30, 31)*
TS Transverse Sinus *(pp. 5, 14, 24, 25, 31–33)*

VENC Velocity Encoding *(pp. 3, 8, 12, 13, 27, 30, 34, 37, 38, 40)*

WMH White Matter Hyper-intensity *(pp. 1, 6, 10, 11)*
WSS Wall Shear Stress *(pp. 2, 3, 7, 15, 16, 25, 34, 38)*

1 Introduction

The first chapter of this thesis serves as an introduction to the theme, providing the necessary background and context for the study. It presents the motivation behind conducting this research and outlines the main goals of the work.

1.1 Context and motivation

The Central Nervous System (CNS) has one of the most abundant blood supplies in the entire human body, with the brain getting around 15% of all the cardiac output. Neurons are the most sensitive cells to oxygen supply interruption, where neuronal death can occur within a few minutes [2]. The brain perfusion is mediated by the cerebral small vessels; therefore they play a crucial role in the health of the brain and its function [2, 3].

Accelerated growth of the rate of cognitive impairment is an emerging problem of the senescent population. Cerebral Small Vessels Disease (CSVD) is a neuropathological condition that affects cerebral arterioles, capillaries, and venules, resulting in the damage of cerebral white and deep grey matter [4]. The increase in life expectancy has led to a prevalence of CSVD, affecting everyone older than 90, causing neurological loss and cognitive decline. It is known that CSVD causes 25% of strokes, 45% of dementia cases, and 70% of vascular dementia cases[5]. Despite being a common disease, CSVD's pathogenesis is still uncertain and a subject of many studies [2], as is the relationship between Cerebral Blood Flow (CBF) and CSVD.

The most reliable imaging diagnostic method for this disease is Magnetic Resonance Imaging (MRI), with a diagnosis based on imaging biomarkers, such as recent subcortical infarcts, White Matter Hyper-intensity (WMH), cerebral microbleeds, and enlarged perivascular spaces [6, 7]. The most recent imaging techniques, which measure blood vessel alterations and blood flow pulsatility, can detect earlier signs of the disease than standard ones, providing an opportunity to mitigate the onset of dangerous symptoms of CSVD and help to better understand the complex relation between vascular and brain health.

The different techniques used in clinical practice to assess flow and perfusion parameters include Computed Tomography (CT) perfusion scan, single-photon emission computed tomography and positron emission tomography. However, all these techniques are invasive since they require the use of exogenous contrast or ionizing radiation [8]. Four-dimensional (4D) Phase-Contrast Magnetic Resonance Imaging (PC-MRI), also known as 4D flow, emerges, as a powerful technique, to overcome these limitations.

Although Two-dimensional (2D) PC-MRI has already been validated to measure velocities in intracranial vessels, 4D flow holds some advantages, including the ability to encode velocity in multiple directions, in a Three-dimensional (3D) volume [9]. As a result of its unidirectional velocity encoding and limited spatial coverage, 2D PC-MRI requires technicians to manually define the cross-sectional plane, making it very error-prone.

Multiple hemodynamic biomarkers, including arterial and venous pulsatility (which can be characterized by Pulsatility Index (PI) and Flow Volume Pulsatility (FVP)), arterial stiffness (characterizable by Wall Shear Stress (WSS) and Pulse Wave Velocity (PWV)), flow rates (characterized by blood flow waveforms) and arterial stenosis (characterizable by Pressure Drop (PD)) can be studied using only a 10 minutes 4D PC-MRI [10] and provide valuable information to understand a lot of brain diseases.

Hence, it is critical to study and validate this technique in order to evaluate the aforementioned parameters.

Cardiac 4D PC-MRI's reproducibility has been studied as well as the extraction of the parameters previously stated, revealing good results [11, 12]. This thesis aims to apply the same methodology, used for main vessels, such as aorta, carotid artery and pulmonary artery, in the context of cerebrovascular 4D flow. This is challenging due to the high spatial resolution required to study such small-sized cerebral vessels.

Although certain research papers revealed good reproducibility results for cerebral 4D PC-MRI, there are no comprehensive studies of CBF employing PI, FVP, WSS, PD, PWV. Thus, this work is important to understand the relationship between the aforementioned biomarkers and the direct measurements of the 4D flow (velocities) as well as to evaluate the accuracy of this technique to estimate them.

1.2 Objectives

This thesis work is part of a project that aims to evaluate and characterize CSVD, via MRI analysis, with the purpose of early diagnosis of the disease.

Ana Duarte, in a previous research work [13], evaluated the test-retest accuracy of 4D PC- MRI data to quantify hemodynamic parameters such as PI, FVP, cross-sectional area, and minimum, maximum, and mean velocities of intracranial arteries. A software tool was also validated for post-processing the data acquired. Ana Duarte concluded, in her work, that velocity values were underestimated which was speculated to be due to an improper imaging scheme used.

Hence, the main goal of this work is to use blood flow information from 4D PC-MRI for the study of brain vascularization. For that, I propose researching the following topics:

- To optimize the parameters, namely the Velocity Encoding (VENC) along the three axes, used in MRI acquisition of both arterial and venous studies;
- To perform a scan-rescan, in 6 weeks time interval, with the optimized parameters of the arterial study, on healthy volunteers;
- To measure the peak, maximum, minimum and mean velocities and vessel's area in both days;
- To analyze statistically the data obtained and to assess the consistency of the methodology;
- To perform an arterial and venous study on healthy volunteers;
- To extract various hemodynamic biomarkers, namely PI, FVP, WSS, PD, PWV;
- To discuss the data obtained, doing a comparison with existing data in the literature.

The research work described in this dissertation was carried out in accordance with the norms established in the ethics code of Universidade Nova de Lisboa. The work described and the material presented in this dissertation, with the exceptions clearly indicated, constitute original work carried out by the author.

2

Theoretical Considerations

This Chapter describes the main concept for the understanding of this thesis. Primarily, the fundamental concepts of anatomy and physiology of the brain's circulatory system.

Once these principles are held, the focus shifts to the Cerebral Small Vessels Disease (CSVD), with an overview of the disease and the relationship between this disease and several hemodynamic biomarkers.

Furthermore, the principles for comprehending the Four-dimensional (4D) Phase-Contrast Magnetic Resonance Imaging (PC-MRI) are presented, so that the physics underlying the data acquired may be better understood.

2.1 Cerebral Blood Flow

As previously stated, the integrity of cerebral vascularization is critical for normal brain functioning and thus for the health of an entire organism. Cerebral Blood Flow (CBF) is one of the most commonly used parameters to evaluate cerebral circulation and it measures the volume of blood passing through $100g$ of tissue per unit time [14].

2.1.1 Anatomy Review

The blood supply to the brain is provided by four principal arteries: the right and left Internal Carotid Artery (ICA) and the right and left vertebral arteries [1]. Each ICA is divided into three branches: ophthalmic artery, anterior cerebral artery, and Middle Carotid Artery (MCA). The vertebral arteries merge to form the Basilar Artery (BA), which is further divided into two branches, the left, and right posterior arteries [15]. The intercommunication of these arteries forms the Willis circle, as illustrated in figure 2.1.

[1] Only those that will be studied in this work appear capitalized for better identification

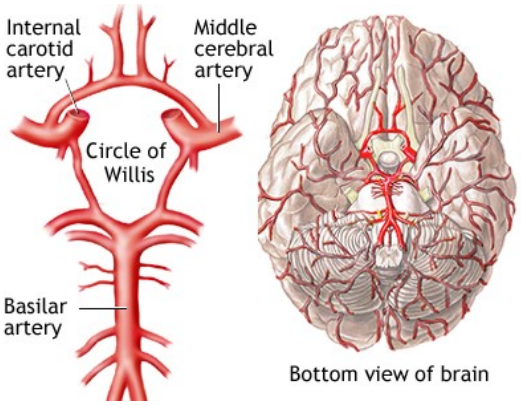

Figure 2.1: Representation of the Circle of Willis and the remain arterial system. Retrieved from [16]

The brain is drained radially, in a centrifugal direction by numerous veins. The venous system can be divided into the superficial and deep systems. The Superior Sagittal Sinus (SSS) and cortical veins, which compose the superficial systems, drain the surface of both cerebral hemispheres. The deep system consists of the Transverse Sinus (TS), straight sinus and sigmoid sinus and functions to drain the deeper surfaces of the cerebral hemispheres. Nearly all of the venous blood from the brain leaves the cranium by way of the Internal Jugular Vein (IJV) [17–20]. It is possible to see an illustration of the cerebral venous system in figure 2.2, as well as a scheme for a better understanding of the deoxygenated blood's draining flow.

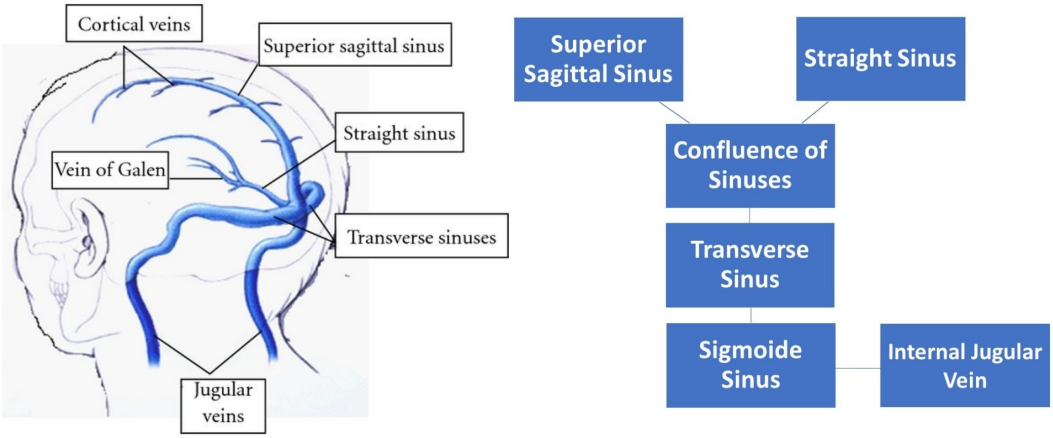

Figure 2.2: Representation of the Brain's Venous System. Retrieved from [21]

At the microcirculation level, where the brain perfusion takes place, we have the capillaries. It has been estimated that nearly every neuron in the human brain has its own capillary, and the total length of brain capillaries is about 400 miles [22].

2.1.2 Physiology Review

The arterial tree is responsible for delivering blood from the left ventricle to the capillaries of various organs and tissues, dampening the pulsations generated by the heart, thereby ensuring a continuous or near-continuous flow of blood through the capillaries [23].

The compliance characteristic of blood vessels plays a crucial role in the regulation of blood flow dynamics. However, as individuals age, the vessels undergo structural changes that lead to a loss of compliance, resulting in increased stiffness. When the vessels become stiff, their ability to dampen the pulsatility of blood flow diminishes [24].

2.2 Cerebral Small Vessels Disease

CSVD is a widely used term to refer to several diseases affecting small arteries, arterioles, venules, and capillaries of the brain and it refers to several pathological processes and aetiologies [25].

There are different types of small vessel diseases: arteriosclerosis (or age-related and vascular risk-factor-related small vessel diseases), sporadic and hereditary cerebral amyloid angiopathy, inherited or genetic small vessel diseases distinct from cerebral amyloid angiopathy, inflammatory and immunologically mediated small vessel diseases, venous collagenases and other small vessels diseases [26].

The structural neuroimaging biomarkers that are usually used to characterise CSVD are: recent small subcortical infarcts that can cause stroke; White Matter Hyper-intensity (WMH) in the periventricular and deep white and grey matter; enlarged perivascular spaces; lacunes; microbleeds; and cerebral atrophy [6, 27].

The risk factors associated with CSVD are age, hypertension, diabetes and smoking [28]. These risk factors lead to structural and functional changes in the arterial wall, resulting in decreased elasticity and increased stiffness of the arteries. As a result, an undamped pulsatile pressure reaches the distal cerebral arteries and microcirculation, resulting in brain damage [29].

Clinical implications of CSVD include intracerebral haemorrhage, which can be manifested by progressive cognitive decline, mood disorders or depression [30], acute ischaemic stroke [31]. The clinical Implications of CSVD go beyond the disease itself since it can worsen the cognitive outcome of Alzheimer's disease and it can increase the risks of parkinsonism [32, 33].

2.2.1 Hemodynamic Biomarkers for brain diseases

It is well-established that as individuals age, the compliance of blood vessels tends to decrease. This decline in compliance can be attributed to various structural changes that occur in the vessel walls. One prominent change is vascular stiffening, which results in the arteries losing their elasticity and flexibility [10, 34, 35].

As consequence, the pulsatility associated with the heartbeat becomes less damped, leading to heightened levels of pulsatility in the distal cerebral vessels. These elevated levels of pulsatility can be quantified using parameters such as the Pulsatility Index (PI) and the Flow Volume Pulsatility (FVP). Another consequence of the arterial stiffening is the increase of the arterial Pulse Wave Velocity (PWV) [10, 36].

Atherosclerosis is often related to arterial stiffening, since the accumulation of plaque and the thickening of the vessel walls contribute to the loss of compliance. Typically, regions characterized with low Wall Shear Stress (WSS) have a higher probability of atherosclerosis formation [10, 37].

Regarding Pressure Drop (PD) is often calculated to assess arterial stenosis and the stroke risk [38].

Alzheimer's Disease is also associated with changes in cardiac-related dynamics in cerebral blood flow. Increased arterial and venous pulsatility and increased PWV, potentially damaging the cerebral microcirculation and indicating higher exposure to hemodynamic stress[39–41].

As was described in the previous section, this brain diseases can be either the cause or a clinical implication of CSVD. Therefore, it is of extreme importance to study these parameters for a better understanding of this disease and to move one step closer to its early diagnosis.

2.3 Magnetic Resonance Imaging

Magnetic Resonance Imaging (MRI) is an imaging technique based on the interactions between nuclear particles, spins, and applied magnetic fields [33].

2.3.1 Magnetic Resonance Angiography

Magnetic Resonance Angiography (MRA) provides a way to visualise and measure the blood flow in the arteries, making use of the motion sensitivity of MRI, created with the use of gradients [42]. The two most common non-contrast MRA techniques are Time-of-Flight MRI, and PC-MRI, which results in hypo and hyper intensification, respectively, of the vessels with the flowing blood [43, 44]. Unlike X-Ray Angiography these techniques are non-invasive.

2.3.1.1 PC-MRI

PC-MRI technique relies on the detection of changes in the phase of blood's transverse magnetization as it moves along a magnetic field gradient. These changes are caused by bipolar gradients, which produce a zero-phase shift for stationary spins and a non-zero phase shift for moving spins. The acquired phase shift increases with the amplitude and duration of the gradients, but it also depends on the velocity of the spins [45, 46].

It is possible to acquire Two-dimensional (2D) or Three-dimensional (3D) images, depending on whether a second phase-encoding gradient is included in the slice selection direction [46].

To study the relation between the phase shift and the velocity, it is necessary to set a parameter called Velocity Encoding (VENC), that corresponds to the maximum velocity that can be encoded by the sequence (ie., associated with a phase shift of 180). [42, 45]. To choose an appropriate VENC is a crucial step in configuring the parameters, since it controls the range of possible flow velocities and impacts the signal-to-noise ratio [47].

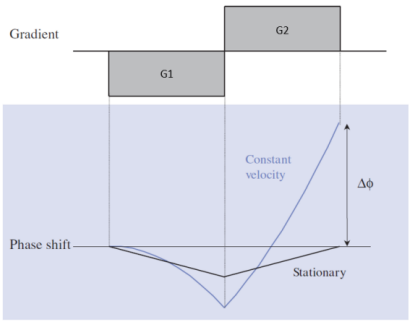

Figure 2.3: Phase shift representation when applied bipolar gradients. Retrieved from [42]

2.3.1.2 4D PC-MRI

PC-MRI data can be acquired from multiple points in the cardiac cycle, in order to produce dynamic angiograms. The electrocardiographic triggering is done retrospectively through gating and data is continually acquired, using pulse peaks and R waves as markers to identify the phase of the cardiac cycle. This technique enables the visualization and quantification of flow throughout the cardiac cycle [46, 48].

4D PC-MRI also called 4D flow is a 3D time-resolved PC-MRI, which implies that velocity encoding is done along three axes, yielding three spatial dimensions, as well as a time dimension since it is performed also throughout a cardiac cycle, as illustrated in figure 2.4 [12, 45, 49]. See, therein, how the R peak, from an electrocardiogram, can be used as a trigger, as stated above.

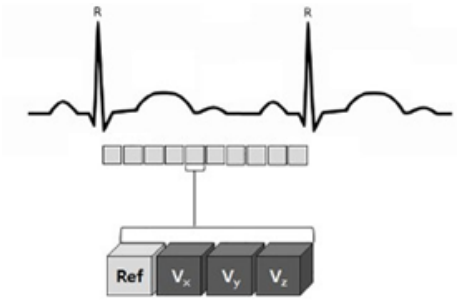

Figure 2.4: Illustration of 4D flow acquired data, Anatomy image the velocity information of each anatomical axes, throughout a cardiac cycle. Retrieved from [45]

3

State of the art

Section 3.1 presents the most recent studies of 4D flow used to evaluate the vascular function. Section 3.2 highlights studies that related CSVD with the same hemodynamic parameters, as well as neuroimaging biomarkers.

3.1 Studies with 4D flow

There is a growing interest in quantifying CBF, and other parameters related to vascular function. Transcranial Doppler (TCD) is a noninvasive technique that provides real-time measurements of intracranial arteries parameters [50], thus it has been widely used to compare and validate the results found with 4D flow MRI.

As previously stated, Ana Duarte's work [13] assessed the test-retest reproducibility of 4D PC-MRI measurements of pulsatility-related indexes, flow, velocity, and anatomical parameters of ICA, MCA and BA. Duarte stated that several values, such as velocities and by extension PI and FVP weren't in agreement with the literature, and that underestimation is, probably due to the imaging sequence and sampling scheme used.

Other studies using 4D flow MRI technique report an underestimation of known velocity values in small vessels. Meckel et al. [9] measure velocities in ICA, BA and MCA and concluded that spatiotemporal averaging effects of 4D PC-MRI may contribute to a vessel diameter-dependent mild velocity underestimation and overestimation in smaller and larger-sized arteries (ICA and BA), respectively.

Ha et al. [51] measured subsegmental velocities, bilaterally, in MCA and BA with 4D flow MRI and TCD. In that research, measurements were underestimated as well. The study's limitations included the fact that the field of view, of the 4D flow MRI, did not include the whole transforaminal window level, which may have caused a bad correlation between TCD and 4D flow MRI at the BA. Another limitation was poor spatial resolution, needed to have access to information at the small-sized intracranial vessels.

A systematic review, carried out by Morgan et al. [52], identified and examined 61 research studies that assessed intracranial vessels using 4D flow, in a total of 2665 subjects. Among all studies considered, Morgan et al. reported that there is a consensus that

4D PC-MRI provides useful data to study intracranial vessels. On the other hand, the constraints mentioned therein point, in general, to high scanning time, meaning that data acquisition has to be traded off against the acquisition time.

Although the 4D flow technique has been widely studied, and shows great potential to quantify CBF, there are still some limitations that need to be addressed.

3.2 Biomarkers for CVSD

CSVD is widely studied, yet there are still uncertainties regarding pathogenesis. And, since this thesis is a component of a larger project with the final objective of applying these methodologies to the study of CSVD, it is important to conduct a comprehensive review of the existing knowledge of this disease.

A systematic review carried out by Shi et al. [53] identified and examined 27 studies that assessed intracranial pulsatility in relation to CSVD features, collected from 3356 subjects. Most data analysed supports a cross-sectional association between CSVD and higher pulsatility, in large intracranial arteries such as MCA and ICA. Nevertheless, Shi et al. concluded it is still not known if high pulsatility leads to more WMH.

Another systematic study concluded that CBF reductions were more severe within WMH compared to normal-appearing white matter in patients with moderate-to-severe WMH burden [54]. Therein Stewart et al. suggest that WMH represent areas of focal perfusion deficits, which are more severe than global hypoperfusion.

Both articles referenced above mention studies within the review where CBF is not seen to be linearly related to CSVD or WMH burden.

Shi et al. [55] in yet another review article, concluded that CBF is lower in regions that developed WMH. Nevertheless, the relation was diminished after non-age matched and dementia patients were excluded, implying that hypoperfusion and low cortical CBF are more likely a result of WMH than its cause.

Nam et al. [56] concluded that increased ipsilateral PI was closely related to CSVD, in particular when associated with WMH and old lacunar infarcts.

To address the heterogeneity of CBF in CSVD patients, a recent study evaluates the relationship between CSVD and CBF [57]. Lu et al. identified three distinct subtypes of CSVD based on their unique CBF patterns. These subtypes were classified based on the observation that CBF may increase in certain regions of the brain while simultaneously decreasing in others within the same subtype of CSVD. The findings presented in the article not only highlight the complex nature of CSVD but also provide a starting point for future research in this field.

In a cross-sectional study [58] involving 89 patients who had experienced acute ischemic stroke or transient ischemic attack, researchers used 4D flow MRI to calculate PI and FVP for the ICA and MCA. Those parameters were then analyzed, to determine their associations with WMH volume, brain volume, and cognitive function. A significant association between FVP, in ICA, and WMH volume, indicates that increased arterial

pulsatility may contribute to the development of WMH. Additionally, both FVP and PI, in MCA, were associated with decreased cognitive function, suggesting that higher arterial pulsatility, in the MCA, may be linked to cognitive impairment in stroke patients.

Chuang et al. [59] investigated the associations between carotid flow velocity, blood pressure, brain volume, and CSVD. The study included 721 adults aged 50 years and above. It included measurements of flow velocities at the common carotid artery and ICA using TCD, and detected CSVD neuroimaging biomarkers on brain MRI. A CSVD score was made based on these biomarkers. The results showed that the CSVD score was negatively associated with grey matter and white matter volumes, but positively associated with systolic blood pressure. End-diastolic velocity, at the common carotid artery, was positively associated with white matter volume and negatively predicted the presence of CSVD.

After reviewing all the analyzed articles, it can be inferred that there are still uncertainties regarding CSVD's relation with CBF, pulsatility and other hemodynamic biomarkers, thus this project is of extreme importance to the comprehension of this disease.

4

Methodology

This Chapter describes the methods used during this project. Section 4.1 presents general information about the participants in the study. In section 4.2 is described, for all studies, the protocols used for image acquisition. Section 4.3 clarifies the software used and the alterations made for data processing as well as the approaches used to get the parameters. This chapter concludes with a description of how the statistical analysis is performed in section 4.4.

4.1 Participants

A total of 9 healthy volunteers, with no history of neurological disease and no contraindications to MRI, participated in this study. Of these recruited individuals (female, n = 5; male, n = 4; mean age, 22.3 ± 2.8 years), two males were excluded from the reproducibility study.

The study protocol was approved by the Medical Ethics Committee of Hospital da Luz and each participant provided signed written informed consent before participation.

4.2 MRI imaging protocol

The 4D PC-MRI acquisitions were conducted on a 3T scanner (Signa Premier, GE Healthcare, Waukesha) equipped with a 48 channel receiver head AIRTM coil.

4.2.1 Pilot Studies

Two pilot investigations were carried out to determine the most suitable VENCs for both arterial and venous studies. The arterial pilot was conducted on 1 individual and 2 VENCs were assessed: 110 *cm/s* and 150 *cm/s*. The venous pilot study, on the other hand, involved 2 volunteers and assessed 3 VENCs: 40 *cm/s*, 60*cm/s* and 100 *cm/s*.

Dr. Pedro Vilela and Eng. Pablo Garcia-Polo assisted in the analysis of the data from the pilot studies, which led to the selection of VENC = 150 *cm/s* and VENC = 60 *cm/s* for arterial and venous studies, respectively.

The selection of appropriate values for the VENC was an important consideration in this study, and it was made taking into account the age and health status of the participants.

Specifically, for the arterial VENC, additional factors were considered since the initial objective was to evaluate the impact of physical activity on vascular function. Therefore, it was anticipated that the acquisition after physical exercise might require a higher VENC setting. This is because physical exercise can lead to increased arterial blood velocities. Yet, due to time constraints, physical exercise was never explored in the current study.

4.2.2 Reproducibility study

To assess the scan-rescan reproducibility of the MRI arterial measurements, seven volunteers were scanned twice, between may and july, with 6-weeks time difference between scans. The imaging parameters were as follows: field of view = 220 *mm*, acquired spatial resolution = 0.9 *mm* × 0.9 *mm* × 0.5 *mm*, acquisition matrix size = 220 x 220, reconstruction matrix size = 256 × 256, repetition time (TR) = 4.6 *ms*, echo time (TE) = 2.7 *ms*, flip angle = 10° and VENC = 150 *cm/s*.

4.2.3 Intracranial Arterial and Venous blood flow study

To carry out this study, all nine volunteers were scanned twice in a row with two different sequences. The arterial sequence's parameters were the same as the ones listed for the reproducibility study.

The venous study used the following imaging parameters: field of view = 220 *mm*, acquisition matrix size = 220 x 220, reconstruction matrix size = 256 × 256, acquired isotropic spatial resolution = 0.9 *mm* × 0.9 *mm* × 0.5 *mm*, repetition time (TR) = 5.1 *ms*, echo time (TE) = 3.1 *ms*, flip angle = 10° and VENC = 60 *cm/s*.

4.3 Data processing and analysis

All the data were analysed using MATLAB 9.13.0 (R2022b), Natick, Massachusetts software [60]. In particular, the 4D flow data processing was performed via 4D Flow PWV Tool, created by Eric Schrauben [61]. In a previous work [13], this tool was adapted to output the maximum, minimum and medium velocities along the cardiac cycle and the vessel's area, these values were obtained from an average over six consecutive centerline voxels of the previously specified locations in the vessels. Mean cross-sectional velocities were used to calculate the aforementioned velocities. The tool was also modified to compute the pulsatility index and the flow volume pulsatility.

The 4D flow analysis was performed using the tool above. In addition to the modifications made by Duarte, the peak velocity of a cross-section was selected and the maximum peak velocity along the cardiac cycle was also outputted. The maximum peak velocity, now called peak velocity, is an average of the values obtained from six consecutive centerline voxels.

4.3.1 Reproducibility study

For each subject, the velocities (maximum velocity, mean velocity, minimum velocity and peak velocity) and vessel's area were measured in bilateral ICAs, bilateral MCAs, and the BA to assess the reproducibility of this methodology. The segments chosen to represent ICA, MCA and BA were, respectively, Cavernous Segment (C3) of ICA, Sphenoidal Segment (M1) of MCA and the middle segment of the BA, as illustrated in figure 4.1.

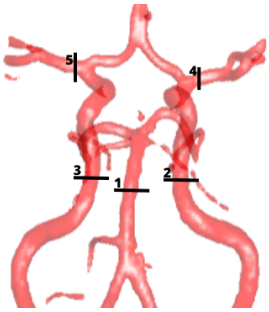

Figure 4.1: Three-dimensional vascular reconstruction of the circle of Willis using the 4D flow PWV Tool [61] on data collected on an example subject. 1 - Basilar artery; 2 - Cavernous segment of the left internal carotid artery; 3 - Cavernous segment of the right internal carotid artery; 4 - Sphenoidal Segment of the left middle cerebral artery; 5 - Sphenoidal Segment of the right middle cerebral artery

4.3.2 Arterial and Venous blood flow study

To conduct a complete study of the intracranial arterial and venous blood flow, several hemodynamic biomarkers were estimated from the velocity information provided by the 4D flow. The measurements of the venous study were conducted on the SSS (1) and right and left TS (2 and 3, respectively), as illustrated in figure 4.2.

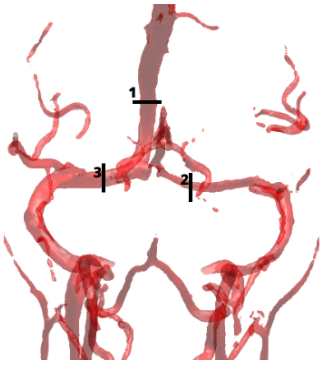

Figure 4.2: Three-dimensional vascular reconstruction of the dural venous sinuses using the 4D flow PWV Tool [61]. 1 - superior sagittal sinus; 2 - left transverse sinus; 3 - right transverse sinus

Flow Rates

Flow rates were estimated for each cross-section by multiplying the area of the blood vessel by the velocity of the blood, estimated over the 30 cardiac frames, resulting in a blood flow waveform. It is important to note that the vessel's area was considered to remain constant throughout the entire cardiac cycle, disregarding its compliance [61].

Arterial and Venous Pulsatility Index

The arterial and venous pulsatility can be described in terms of indexes based on systolic and diastolic velocities [10]. Measurements of the PI were obtained via equation 4.1.

$$PI = \frac{Q_{syst} - Q_{diast}}{Q_{mean}}, \tag{4.1}$$

where Q_{syst}, Q_{diast} and Q_{mean} represent the systolic, diastolic and mean flow, respectively. These flows are calculated by multiplying the maximum, minimum and mean velocity by the vessel's area [13].

Flow Volume Pulsatility

In order to calculate the FVP, Duarte [13] followed several steps. Firstly, the mean flow was subtracted from the flow waveform, resulting in a waveform that represents the pulsatile component of the flow. Next, the cumulative integral of this remaining waveform was obtained, capturing the cumulative volume changes over time.

The FVP was quantified as the difference between the maximum and minimum values of the vertically shifted curve, that aligned the minimum volume with zero [13]. In figure 4.3 is illustrated this curve, where ΔV represents FVP

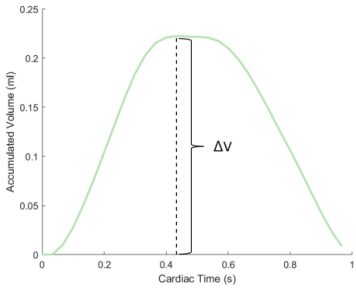

Figure 4.3: Cumulative volume changes over a cardiac cycle, curve shifted towards zero. Retrieved from [13]

The FVP was calculated for the arterial vessels, namely ICAs, BA and MCAs, since FVP is a measure of the pulsatile component of the arterial load.

Wall Shear Stress

Analysing the velocity from the arterial wall, which is zero, to the middle of the artery, which is the peak velocity, the WSS can be estimated by using the steepness of the velocity

increase [10]. More specifically, it was calculated by multiplying this steepness by the blood's viscosity, considered as3.2×10^{-3} $Pa{\cdot}s$ [62].

Figure 4.4 illustrates the velocity profile on various cutplanes of the left carotid artery. As previously mentioned, the figure provides visual confirmation that the velocity increases as the distance from the center of the cutplane decreases.

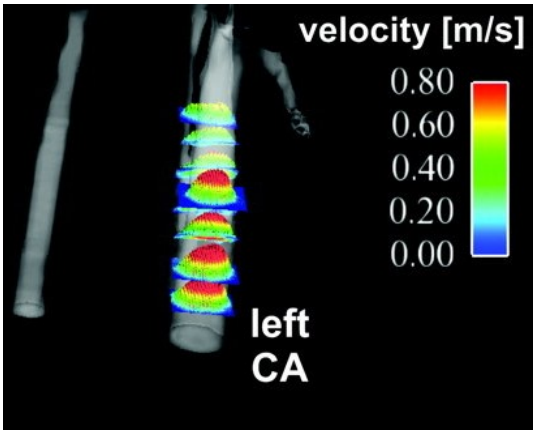

Figure 4.4: Velocity profile on left carotid artery cutplanes. Adapted from [63]

In addition to the extraction of the WSS for a specific cutplane, WSS was also expressed as a function of arterial segments [63].

Pulse Wave Velocity

To calculate PWV, Schrauben et al. [61] used a complex wavelet cross-spectrum analysis. This method enables temporal localization of signal frequencies, to estimate transit time. Then local PWV is calculated as the ratio between segment length and the estimated value for transit time [64].

This methodology, employed by Schrauben et al. [61] and developed by Bargiotas et. al [64], is thoroughly described in [64].

In this thesis, the PWV were computed across the intracranial ICA segment.

Pressure Drop

The PD was estimated using the Bernoulli Principle, which is described by the equation 4.2.

$$PD = 4v_2^2 \times \left(1 - \left(\frac{A_2}{A_1}\right)^2\right) \tag{4.2}$$

This approximation is commonly used when there is a stenosis, so that the degree of the stenosis can be evaluated, where A_1 is the vessel's area proximal to the stenosis, A_2 is the vessel's area at the stenosis and v_2 is the blood's velocity at the stenosis.

In this thesis, the PD was calculated using 2 sites of the same vessel or 2 sites of different vessels linked by a bifurcation. In both cases, A_1 is the vessel's area of the proximal site, A_2 is the vessel's area of the distal site and v_2 is the blood's velocity at the distal site.

In figure 4.5 is illustrated and summarized the pairs of sites, for center and right side of the circle of Willis. Analogously to the right, the values for PD on left side were calculated.

Site 1	Site 2
Proximal BA (1)	Distal BA (2)
Proximal ICA (3)	Distal ICA (4)
Distal ICA (4)	Proximal MCA (5)

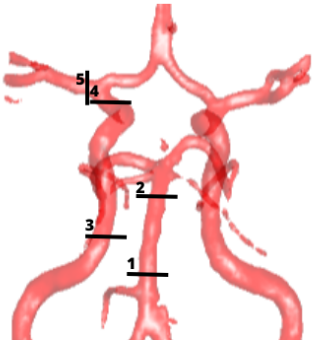

Figure 4.5: Pair of sites used to calculate pressure drops. 1 - Proximal site of the basilar artery (BA); 2 - Distal site of the basilar artery (BA); 3 - Proximal site of the internal carotid artery (ICA), 4 - Distal site of the internal carotid artery (ICA); 5 - Proximal site of the middle cerebral artery (MCA)

Total Blood inflow and outflow

To calculate the total cerebral blood inflow, the mean blood flow across a cardiac cycle of the basilar artery (BA) and the right and left internal carotid arteries (ICA) were summed, as described by Dunaas et al. [65].

Similarly, the total cerebral blood outflow should be calculated by summing the mean blood flow across the cardiac time of the right and left IJV. However, due to difficulties in accessing the IJV directly, an alternative approach was adopted. The outflow was instead calculated using data at the bilateral Sigmoid Sinus (SS), as illustrated in Figure 4.6.

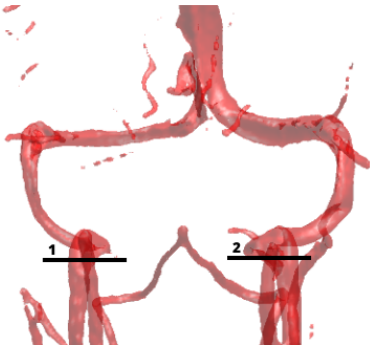

Figure 4.6: Three-dimensional vascular reconstruction of the dural venous sinuses using the 4D flow PWV Tool [61]. 1 - right sigmoid sinus; 2 - left sigmoid sinus

This decision to use the SSs for outflow calculation was based on practical considerations and anatomical relationship between the inferior petrosal sinuses and the SSs, which

together form the IJV. While the direct measurement of IJV flow would have been ideal, the use of the SSs provides a reasonable approximation for the venous outflow from the brain.

4.4 Statistical Analysis

Statistical analyses were performed using IBM's SPSS Statistics 29.0.1.0 software (IBM, Armonk, NY) and Python's library Matplolib [66].

All results of the measurements and calculations values were reported as mean ± standard deviation fairs. The normality of the data was analysed using the Shapiro-Wilk test. The interpretation of this test is as follows: if the p-value > 0.05, there is insufficient evidence to reject the null hypothesis, which suggests that the data can be reasonably assumed to follow a normal distribution. On the other hand, if the p-value < 0.05, there is evidence to reject the null hypothesis, indicating that the data deviates from a normal distribution.

To assess reproducibility, Pearson Correlation Coefficient (r), and Intraclass Correlation Coefficient (ICC) were calculated. The ICC and their 95% Confident Interval (CI) were calculated based on a single rating, absolute-agreement, 2-way mixed-effects model (ICC(2,1)).

The r and ICC were classified as: poor (<0.50), moderate (0.50–0.69), good (0.70–0.84), very good (0.85–0.94), and excellent (≥0.95). A p-value ≤ 0.05 was considered statistically significant.

The characteristic differences within the healthy subject cohort were evaluated with the Paired t-Test. A p-value ≤ 0.05 was considered statistically significant and indicates that there is a significant difference between the paired observations in both samples.

Bland-Altman plots and analyses were used to assess the agreement between measurements carried out on both days. A Mean Relative Difference (MD) (the difference between the two measurements, divided by the mean of the measurements) inferior to 5% was considered a satisfactory result. To compute the Bland-Altman plots, and allow comparison across subjects, the relative difference was plotted against the average of the two measurements. The Limits of agreement (LoA) were calculated as mean ±1.96 times the relative standard deviation.

5

Results

Within this chapter, the findings derived from the study are presented and scrutinized.

Firstly, the results of the reproducibility study are expounded upon to ensure the accuracy associated with the 4D flow technique. Additionally, the results of the extracted parameters are presented.

5.1 Reproducibility Study

5.1.1 Descriptive Statistics

The scan-rescan results (Day 1 and Day2) pertaining velocities and vessel's cross-sectional area, for all examined arteries are presented in tables 5.1 and 5.2, as mean ± standard deviation.

Table 5.1: Mean and standard deviation of the velocities (minimum, maximum and mean) for all arteries analysed on both Day 1 and Day 2

Vessel	$\mathbf{V_{min}}$ (cm/s)		$\mathbf{V_{max}}$ (cm/s)		$\mathbf{V_{mean}}$ (cm/s)	
	Day 1	Day 2	Day 1	Day 2	Day 1	Day 2
BA	29.5 ± 5.2	28.5 ± 4.2	48.9 ± 7.3	49.4 ± 7.9	39.5 ± 6.5	37.9 ± 5.3
l ICA	23.9 ± 5.0	23.6 ± 3.7	43.6 ± 8.8	43.8 ± 7.8	33.3 ± 6.7	32.3 ± 5.5
r ICA	21.7 ± 2.8	22.4 ± 3.4	39.4 ± 6.6	42.4 ± 7.6	30.1 ± 4.4	30.7 ± 4.9
l MCA	29.7 ± 5.3	28.8 ± 7.2	53.2 ± 13.0	53.2 ± 12.3	41.4 ± 9.5	39.5 ± 9.3
r MCA	31.0 ± 3.7	30.8 ± 5.6	54.5 ± 8.3	55.1 ± 7.0	42.8 ± 6.3	42.0 ± 6.9

BA = Basilar Artery; **l ICA** = left Internal Carotid Artery; **r ICA** = right Internal Carotid Artery; **l MCA** = left Middle Cerebral Artery; **r MCA** = right Middle Cerebral Artery;

Table 5.2: Mean and standard deviation of the peak velocity and vessel's cross-sectional area for all arteries analysed on both Day 1 and Day 2

Vessel	**Area** (mm^2)		$\mathbf{V_{peak}}$ (cm/s)	
	Day 1	Day 2	Day 1	Day 2
BA	7.1 ± 1.9	6.5 ± 0.7	67.7 ± 16.7	65.7 ± 12.2
l ICA	13.4 ± 1.4	14.2 ± 1.9	64.0 ± 14.9	63.6 ± 14.4
r ICA	14.2 ± 2.9	14.0 ± 2.7	56.4 ± 9.2	59.9 ± 12.1
l MCA	8.9 ± 2.4	10.3 ± 2.4	86.6 ± 25.7	96.5 ± 28.3
r MCA	8.6 ± 2.1	8.9 ± 1.2	84.1 ± 8.3	85.5 ± 15.3

BA = Basilar Artery; **l ICA** = left Internal Carotid Artery; **r ICA** = right Internal Carotid Artery; **l MCA** = left Middle Cerebral Artery; **r MCA** = right Middle Cerebral Artery

To evaluate the normality of the data, the Shapiro-Wilk test was employed. Although some p-values were found to be less than 0.05, the results can be found in I, the null hypothesis of normality was not rejected, what led to the conclusion that the data is normally distributed.

This finding has important implications for subsequent statistical analyses, as many parametric tests and correlations rely on the assumption of data following a normal distribution.

5.1.2 Intraclass Correlation

Assessment of reproducibility was performed using Intraclass Correlation. The summary of ICCs and CIs is presented in tables 5.3 and 5.4.

Table 5.3: Intraclass Correlation Coefficients (ICC) and 95% Confidence Intervals (CI) for minimum, maximum and mean velocities

Vessel	$\mathbf{V_{min}}$		$\mathbf{V_{max}}$		$\mathbf{V_{min}}$	
	ICC	95%CI	ICC	95%CI	ICC	95%CI
BA	0.704	(−0.01 - 0.942)	0.855	(0.359 - 0.974)	0.744	(−0.715 - 0.781)
l ICA	0.811	(0.211 - 0.965)	0.878	(0.433 - 0.978)	0.854	(0.343 - 0.970)
r ICA	0.724	(0.051 - 946)	0.814	(0.285 - 0.965)	0.877	(0.462 - 0.978)
l MCA	0.931	(0.684 - 0.987)	0.924	(0.615 - 0.987)	0.974	(0.653 - 0.996)
r MCA	0.828	(0.263 - 0.969)	0.848	(0.334 - 0.972)	0.766	(0.125 - 0.956)

BA = Basilar Artery; **l ICA** = left Internal Carotid Artery; **r ICA** = right Internal Carotid Artery; **l MCA** = left Middle Cerebral Artery; **r MCA** = right Middle Cerebral Artery;

Table 5.4: Intraclass Correlation Coefficients (ICC) and 95% Confidence Intervals (CI) for vessel's cross-sectional area and peak velocity

Vessel	**Area**		$\mathbf{V_{peak}}$	
	ICC	95%CI	ICC	95%CI
BA	0.144	(−0.715 - 0.781)	0.788	(0.149 - 0.960)
l ICA	0.622	(−0.053 - 0.920)	0.854	(0.515 - 0.987)
r ICA	0.883	(0.494 - 0.979)	0.833	(0.368 - 0.969)
l MCA	0.674	(0,036 - 0,933)	0.763	(0,201 - 0,954)
r MCA	0.225	(−0.70 - 0.825)	0.342	(−0.636 - 0.853)

BA = Basilar Artery; **l ICA** = left Internal Carotid Artery; **r ICA** = right Internal Carotid Artery; **l MCA** = left Middle Cerebral Artery; **r MCA** = right Middle Cerebral Artery

Interpretation

Based on these results, the following conclusions can be drawn:

- BA shows good to very good reproducibility for all parameters except for vessel's cross-sectional area, where ICC was 0.144, which demonstrates poor reproducibility. CI the values are relatively wide, suggesting a poor level of precision in the reproducibility estimates;
- Left ICA shows good to very good reproducibility for all parameters except for vessel's cross-sectional area, where ICC was 0.622, which demonstrates moderate reproducibility. The same goes to CI interval, where the widest interval is the one concerning the vessel's cross-sectional area;
- Right ICA shows good to very good reproducibility for all parameters. The CI values for all parameters are relatively narrow, suggesting a high level of precision in the reproducibility estimates.;
- Left MCA shows good to very good reproducibility for all parameters except for vessel's cross-sectional area, where ICC was 0.674, which demonstrates moderate reproducibility. The same goes to CI interval, where the widest interval is the one concerning the vessel's cross-sectional area;
- Right MCA shows good to very good reproducibility for all parameters except for vessel's cross-sectional area and peak velocity, where ICC was 0.225 and 0.342, respectively, which demonstrates poor reproducibility. The CI intervals for parameters with good reproducibility are narrow, while the vessel's cross-sectional area and the peak velocity are wider.

5.1.3 Pearson Correlation

The Pearson Correlation results, including Pearson Correlation Coefficient (r) and p-value, are summarized in table I.1.

Table 5.5: Pearson Correlation Coefficients (r) and p-values (p) for all parameters (minimum, maximum, mean, peak velocities and vessel's cross-sectional area)

Vessel	$\mathbf{V_{min}}$		$\mathbf{V_{max}}$		$\mathbf{V_{mean}}$		**Area**		V_{peak}	
	r	p	r	p	r	p	r	p	r	p
BA	0.879	0.009	0.837	0.019	0.75	0.52	0.267	0.563	0.370	0.414
l ICA	0.825	0.022	0.867	0.012	0.840	0.018	0.672	0.098	0.835	0.019
r ICA	0.724	0.066	0.860	0.013	0.871	0.011	0.878	0.009	0.882	0.009
l MCA	0.971	0.000	0.914	0.004	0.987	0.000	0.727	0.064	0.781	0.038
r MCA	0.879	0.009	0.837	0.019	0.750	0.052	0.267	0.563	0.370	0.414

BA = Basilar Artery; **l ICA** = left Internal Carotid Artery; **r ICA** = right Internal Carotid Artery; **l MCA** = left Middle Cerebral Artery; **r MCA** = right Middle Cerebral Artery;

Interpretation

Analyzing the results it is possible to infer that:

- BA shows very good and good results for minimum and maximum velocities, respectively. For the remaining parameters, the p-value > 0.05, which identifies lack of statistical significance;
- Left ICA shows good to very good results for all parameters except for vessel's area, where r is 0.672 and p-value > 0.05;
- Right ICA shows very good results for all parameters except for the minimum velocity values, where p-value > 0.05;
- Left MCA shows good to excellent results for all parameters except for vessel's area, where r was 0.727 and p-value > 0.05;
- Right MCA shows very good and good results for minimum and maximum velocities, respectively. For the remaining parameters the p-value>0.05.

5.1.4 Paired t-Test

Paired samples t-Test is used to determine if there is a significant difference between the paired observations in two samples.

The p-values' results for the paired t-Test, for all parameters analysed, across all arteries are listed in table 5.6.

Table 5.6: *p*-values' results of the paired t-Test for all parameters (minimum, maximum, mean, peak velocities and vessel's cross-sectional area)

Vessel	V_{mean}	V_{mean}	V_{mean}	Area	V_{peak}
BA	0.568	0.785	0.429	0.527	0.794
l ICA	0.830	0.909	0.531	0.252	0.908
r ICA	0.514	0.133	0.608	0.527	0.222
l MCA	0.440	0.998	0.027	0.132	0.254
r MCA	0.869	0.802	0.611	0.729	0.833

BA = Basilar Artery; **l ICA** = left Internal Carotid Artery; **r ICA** = right Internal Carotid Artery; **l MCA** = left Middle Cerebral Artery; **r MCA** = right Middle Cerebral Artery;

Interpretation

It is possible to conclude that all *p*-values are higher than 0.05, except the mean velocity of the left ICA, which means that there is no significant difference between the measurements made for each day.

5.1.5 Bland-Altman Analysis

The Bland-Altman plot was used to assess the agreement between the scan and the rescan of all parameters. The mean differences for all parameters are summarized in table 5.7, figure I.1 shows the Bland-Altman plots of BA's cross-sectional area (left) and left ICA's peak velocity (right).

Table 5.7: Relative Mean Difference (%) for all parameters (minimum, maximum, mean, peak velocities and vessel's cross-sectional area)

Vessel	V_{mean}	V_{mean}	V_{mean}	Area	V_{peak}
BA	11.4	8.2	10.9	16.9	12.2
l ICA	10	9.4	10.6	11.3	15.1
r ICA	8.3	10.2	6.1	8.9	8.9
l MCA	9.9	8.7	6.2	17.0	15.1
r MCA	10.0	7.8	9.5	22.1	17.6

BA = Basilar Artery; **l ICA** = left Internal Carotid Artery; **r ICA** = right Internal Carotid Artery; **l MCA** = left Middle Cerebral Artery; **r MCA** = right Middle Cerebral Artery;

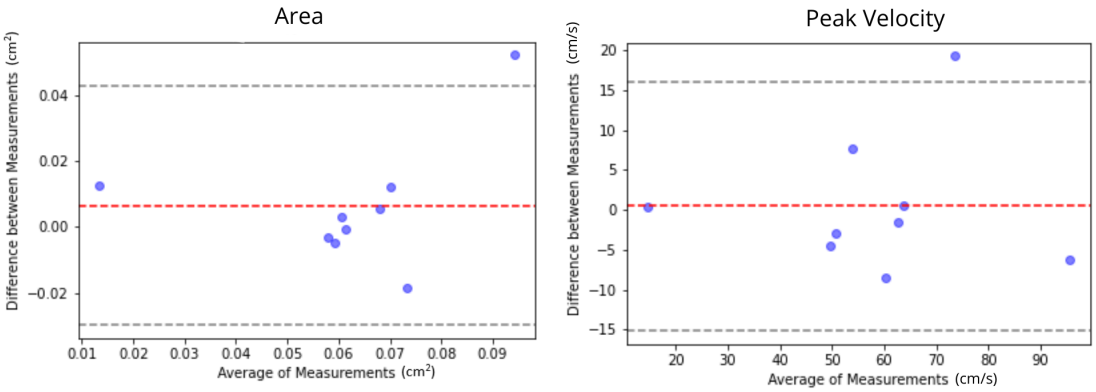

Figure 5.1: Bland-Altman. **Left**: Bland-Altman plot for BA's cross-sectional area. **Righ**:Bland-Altman plot for ICA's peak velocity

Interpretation

It is possible to observe in table 5.7 that there is no MD < 5%, which leads to the conclusion that this analysis had no satisfactory results. Also, figure 5.1 reveal the presence of outliers and wide intervals of the LoA. This observation aligns with the poor results presented in table 5.7.

5.2 Arterial and Venous blood flow study

As was described in 4.2.3, a serie of hemodynamic biomarkers were computed from the 4D flow data-. The arterial parameters were the results of calculations using the measurements acquired in the reproducibility study, namely minimum, maximum, mean and peak velocities and vessel's area. The venous parameters are the result of calculations using the 4D flow venous study's data. The results of these calculations, and the venous data extracted from 4D flow venous study (blood's velocity in the main sinuses and its area) are summarized as mean ± standard deviation in the next paragraphs.

The velocity and vessel's area values acquired for the right and left TS and for SSS are listed in table 5.8

Table 5.8: Mean and standard deviation of the minimum, maximum, mean and peak velocities and vessels cross-sectional area for all the sinuses analysed

Vessel	$\mathbf{V_{min}}$ *(cm/s)*	$\mathbf{V_{max}}$ *(cm/s)*	$\mathbf{V_{mean}}$ *(cm/s)*	**Area** *(mm)*	$\mathbf{V_{peak}}$ *(cm/s)*
SSS	3.6 ± 1.1	4.5 ± 1.4	4.1 ± 1.2	36.8 ± 8.7	12,4 ± 2.1
l TS	5.1 ± 2.3	6.2 ± 2.6	5.7 ± 2.4	27.5 ± 10.0	18,4 ± 4.5
r TS	8.4 ± 3.5	10.1 ± 3.2	9,4 ± 3.4	40.9 ± 16.7	22,5 ± 6.6

SSS = Superior Sagittal Sinus; **l TS** = left Transverse Sinus; **r ICA** = right Transverse Sinus

To analyze flow rates, blood flow waveforms were computed. Figure 5.2 displays a series of blood flow waveforms, obtained from the segment, identified in figure 4.1, corresponding to the right ICA.

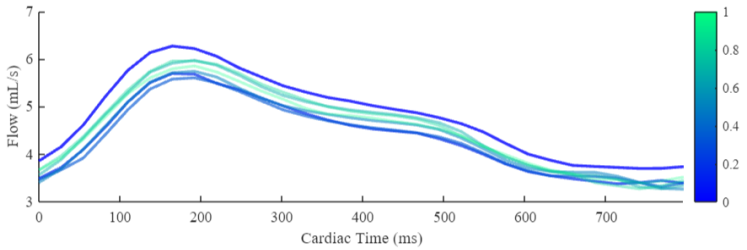

Figure 5.2: Blood flow waveforms for the cavernous segment of the right internal carotid artery

Similarly, figure 5.3 shows a series of blood flow waveforms along the segment identified in figure 4.2 of the right TS. These waveforms illustrate the pulsatile nature of blood flow in this specific segment, capturing the changes in flow rate over a full cardiac cycle.

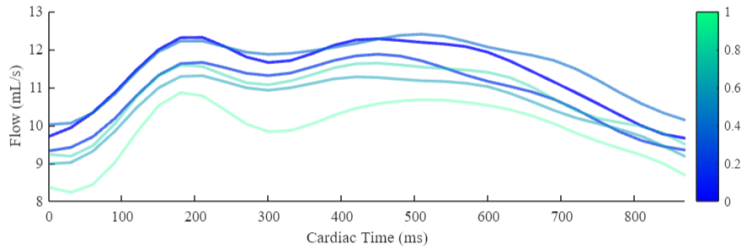

Figure 5.3: Blood flow waveforms for the right transverse< sinus' segment

Table 5.9 lists the results of PI, FVP and WSS for each vessel.

Table 5.9: Mean and standard deviation Pulsatility Index (PI), Flow Volume Pulsatility (FVP) and Wall Shear Stress (WSS) for all the arteries analysed

Vessel	PI	FVP *(ml)*	WSS *(Pa)*
BA	0,56 ± 0,08	0,26 ± 0,15	1,80 ± 0,31
l ICA	0,61 ± 0,08	0,39 ± 0,10	1,28 ± 0,30
r ICA	0,63 ± 0,12	0,38 ± 0,08	1,33 ± 0,56
l MCA	0,63 ± 0,12	0,34 ± 0,12	1,76 ± 0,59
r MCA	0,56 ± 0,10	0,30 ± 0,06	2,06 ± 0,61

BA = Basilar Artery; **l ICA** = left Internal Carotid Artery; **r ICA** = right Internal Carotid Artery; **l MCA** = left Middle Cerebral Artery; **r MCA** = right Middle Cerebral Artery;

As stated in Chapter 4, venous pulsatility was also extracted, and the PI results were as follows: 0.36 ± 0.13 for the SSS; 0.38 ± 0.13 for the TS; and 0.28 ± 0.09 for the right TS.

Moving to the PWV across the intracranial segment of the ICA, the values obtained were; 4.8 ± 2.4 *m/s*, for the left ICA; and 5.2 ± 2.6 *m/s*, for the right ICA.

The PD values obtained were: 0.31 ± 0.16 *mmHg*, for the BA segment, 0.41 ± 0.24 *mmHg*, for the right ICA segment; 0.76 ± 0.63 *mmHg*, for the right ICA-MCA segment; 0.39 ± 0.26 *mmHg*, for the left ICA segment; and 0.63 ± 0.40 *mmHg*, for the left ICA-MCA segment.

Furthermore, the mean ± standard deviation of cerebral blood inflow and outflow were 592.6 ± 82.6 *ml/min* and 326.6 ± 76.2 *ml/min*, respectively.

6

Discussion

In this chapter, we will delve into the results that were presented in the previous chapter. To facilitate a more comprehensive discussion, this chapter will be divided into two sections. The first will focus on the results of the reproducibility study, while the second will compare this work's findings with those of other studies.

6.1 Reproducibility Study

6.1.1 Intraclass Correlation

As was stated earlier, ICC is a statistical measure, which can be used to assess the agreement between measurements.

The analysis of ICC revealed that the maximum velocity yielded the best results compared to other measurements, with a mean ICC of 0.864, indicating a very good level of reproducibility.

On the other hand, the vessel's cross-sectional area showed the worst results, with a mean ICC of 0.510, indicating a moderate level of reproducibility.

Those findings contrast with the study conducted by Duarte [13], in which the optimal parameter was found to be the vessel's cross-sectional area. This discrepancy can be associated with the impact of a higher VENC, that reduces the signal-to-noise ratio, which affects the segmentation of the cross-sectional area of the vessels. As observed in figure 6.1, the vessel cross-sectional area segmentation is being overestimated due to the presence of high levels of noise. This can affect the reproducibility of these measurements.

Although the maximum, minimum, and mean velocities yielded promising results, in the ICC analysis, the assessment of peak velocity proved to be less reliable. This disparity can be attributed to the possibility of noise peaks masking the true peak velocity values. In contrast, the maximum, minimum, and mean velocities are calculated by averaging over a substantial number of voxels, ensuring a more representative and accurate measurement.

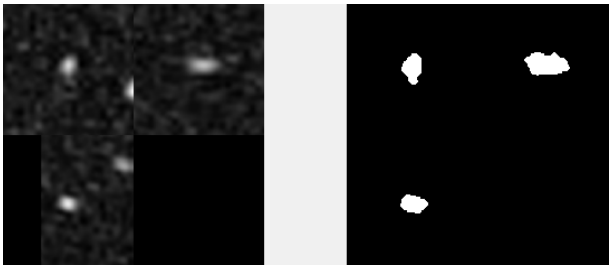

Figure 6.1: Cross-sectional area's segmentation of a Middle Cerebral Artery **Left**: Complex difference (angio) images of the vessel cross-section. **Right:** Respective segmentation

Regarding each vessel, right ICA yields the best results with a mean ICC of 0.853, indicating very good reproducibility. On the other hand, the right MCA showed the worst ones, with a mean ICC of 0.602, representing moderate reproducibility. The reason behind this difference can be ascribed to the fact that MCA is a smaller and more tortuous artery, making it more susceptible to low signal-to-noise ratio effects.

The overall results for ICC analysis were satisfactory for maximum, minimum and mean velocity. Peak velocity ICC analysis showed poor results only for the right MCA. On the other hand, when examining the ICC results for vessel's cross-sectional area, only right ICA revealed very good results, while the remaining vessels displayed poor to moderate results.

6.1.2 Pearson Correlation

To assess the correlation between day 1 and day 2 measurements, it was decided to calculate Pearson the correlation coefficient. The obtained results exhibit similarities to those obtained from the ICC, albeit slightly higher due to the ICC's consideration of both correlation and agreement between measurements.

Among the parameters measured, minimum velocity exhibited the most favourable outcomes, displaying a mean r of 0.856, indicating a high level of reliability.

On the other hand, vessel's cross-sectional area yielded the least satisfactory results, with a mean r of 0.562 and a p-value greater than 0.05, suggesting lack of reliability in the measurements taken for this particular parameter.

These results are consistent with the findings reported for the ICC analysis and the reasons behind them have been thoroughly examined and explained in the preceding section.

Regarding specific vessels, the left MCA demonstrated superior results, with a mean r of 0.876, surpassing all other vessels. Conversely, both the BA and right MCA exhibited the poorest outcomes, with a mean r of 0.621 and a p-value greater than 0.05, indicating a lack of reliability.

Both left and right MCA revealed, respectively, good and bad results. The poor outcome can be attributed to the artery's small and tortuous nature, as mentioned in the previous

subsection. This observation is further supported by the excellent results observed in both right and left ICAs.

The overall poor performance of BA can be primarily attributed to the cross-sectional area of the vessel, as all other parameters exhibit an ICC value greater than 0.7. Upon a thorough analysis of the cross-sectional area measurements for BA in each volunteer, it becomes evident that there is an outlier. Specifically, one of the volunteers had a measurement on day 1 that was twice the magnitude of the measurement on day 2, indicating a significant discrepancy of 6 *mm* between measurements. Due to the small number of elements involved, even a single outlier can have a significant impact on overall results. Therefore, it is crucial to address and account for such discrepancies, in order to obtain more accurate and reliable data.

6.1.3 Paired t-Test

To further assess the agreement between measurements, a Paired t-Test was conducted.

It was possible to conclude that all parameters exhibited no significant difference between the measurements on each day, except the mean velocity of the left ICA.

For a better understanding of this result, the measurements for each volunteer were considered. The largest difference observed between the measurements on both days were approximately 7 *cm/s*. Although this difference is statistically significant, it could be attributed to physiological factors, such as increased heart rate [67] or cerebral vasoconstriction [68].

The Paired t-Test test evaluates not only whether the median difference value is equal to zero but also whether the number of positive and negative differences is balanced. In the case of the mean velocity in the left ICA, there are 5 positive differences and 2 negative differences. When considering this difference, the Paired t-Test yields a low p-value, indicating a significant imbalance between positive and negative differences.

6.1.4 Bland-Altman Analysis

To test the agreement between the results of the measurements, relative differences were compared to the mean values of each measurement acquired, throughout the two days in a Bland-Altman plot. Additionally, the LoA was computed and plotted.

The Bland-Altman Analysis yielded the poorest results among all the analyses conducted. None of the parameters in any of the vessels exhibited a mean difference below 5%. However, upon examining the plots in figure I.1, it becomes evident that this lack of significant difference is primarily due to the presence of outliers, in a rather low dimension of cohort size.

Furthermore, a closer examination of the Bland-Altman plot reveals that the results are influenced by random errors, as indicated by the dispersed distribution of points across the graph. Several factors contribute to these findings. Firstly, as previously mentioned, the small cohort size magnifies the impact of outliers, rendering them more influential in

the analysis. Additionally, the presence of random errors can be attributed to noise, which is understandable given that the high VENC affects negatively the signal-to-noise ratio.

6.2 Comparison with other studies

6.2.1 Arterial Velocities

Table 6.1 includes some of the arterial blood velocities that have been published for arterial blood's velocity. These results were obtained using 2D PC-MRI, 4D PC-MRI and TCD techniques on healthy individuals.

Table 6.1: Mean and standard deviation of maximum, mean, and peak velocity values reported in the literature

Parameter	**BA**	**ICA**	**MCA**
$\mathbf{V_{max}}$ (cm/s)	42 ± 10 to 54 ± 13 [69]	36 ± 5 to 40 ± 6 [70]	49 ± 5 to 62 ± 12 [69, 70]
$\mathbf{V_{mean}}$ (cm/s)	31 ± 7 to 32 ± 7 [71]	25 ± 7 to 35 ± 5 [71]	–
$\mathbf{V_{peak}}$ (cm/s)	61 ± 11 to 78 ± 19 [9]	70 ± 10 to 83 ± 12 [9]	79 ± 18 to 115 ± 20 [9, 51]

BA = Basilar Artery; **ICA** = Internal Carotid Artery; **MCA** = Middle Cerebral Artery

Revisiting tables 5.1 and 5.2, it is possible to state that the values obtained for maximum velocity, in both MCA and BA, fall within the range specified in 6.1. However, the maximum velocity for ICA, observed in the current research is slightly higher, albeit within an acceptable margin.

Regarding mean velocity, ICA exhibited values within the specified interval. In contrast, the values acquired for BA in this thesis are substantially higher.

Furthermore, the peak velocity for both BA and MCA lie within the interval reported in the literature. Yet, ICA shows lower values compared to those listed in table 6.1.

Concerning minimum velocity, no values equivalent to the ones reported in this work were found. In the researches conducted by Meckel et al. [9] and Ha et al. [51], the minimum velocity reported was, actually, the maximum velocity at the end diastole. In this work, the minimum velocity corresponds to the mean velocity at the end diastole.

To ensure a reliable comparison, the maximum velocity at the end of the diastole was extracted, following the methodology used for peak velocity, as stated in subsection 4.3. The results obtained were as follows: BA 50.0±8.9 cm/s; left ICA 40.1±8.1 cm/s; right ICA 36.6±9.7 cm/s; left MCA 49.8±9.3 cm/s; right ICA 50.4±10.8 cm/s. In the aforementioned studies [9, 51], the reported values were: 32.7 cm/s, for BA; 35.5 ± 6.0 cm/s, for ICA; and 41.7 ± 8.8 cm/s, for MCA. The values obtained in this study are higher, specially the ones for BA and MCA. Nevertheless, it is worth mentioning, as stated in Section 3.1, that both studies [9, 51] concluded that their measured velocities were underestimated.

In contrast to Duarte's study, which found an underestimation of velocities, when compared to other studies, the majority of the measurements in this work fell within the range of values reported in the literature or were slightly higher.

The values that exceeded the range indicated by the literature can be explained by what has been discussed in subsection 6.1.1. It is possible that noise peaks are masking true peak velocity values, leading to slightly higher measurements than expected.

Regarding ICA peak velocity, it was found to be slightly underestimated in this study. This can be easily justified by considering the specific segment that was measured. Meckel et al. [9] focused on the ICA siphon, which typically exhibits higher velocities when compared to the segment studied in this work. To support this explanation, three measurements were taken at both sites of the same right ICA, yielding the following values: 70.21 *cm/s*, 75.75 *cm/s*, and 51.11 *cm/s* at the siphon segment, and 50.37 *cm/s*, 60.91 *cm/s*, and 41.50 *cm/s* at the segment studied in this work. These measurements, clearly, demonstrate how the segment being analyzed influences velocity estimates and why the values in the present study are slightly underestimated when compared with Meckel et al. [9].

6.2.2 Venous Velocities

Baumgartner et al. and Stolz et al. [72, 73] used TCD data and found peak velocities of $10 \pm 4\ cm/s$ and $18 \pm 9\ cm/s$ for the SSS and TS, respectively. In a 4D flow study [70] that assessed a slightly higher blood velocity in SSS, with values ranging from $25.2 \pm 4.9\ cm/s$ to $26.1 \pm 4.6\ cm/s$.

The peak velocity values for the venous sinuses obtained in this study, as summarized in table 5.8, are consistent with those reported in previous studies [70, 72, 73].

No studies reporting the minimum, maximum, and mean velocity values in the venous sinuses were found in the literature.

Regarding venous velocities, the values obtained were within the range reported in the literature. However, an interesting observation was made regarding the right side of TS, which exhibited a noticeably higher velocity, when compared to the left side, with a significant difference of 4 *cm/s*. This finding prompted further investigation into the potential physiological causes behind this discrepancy.

To delve deeper into this relatively significant difference, each candidate was examined individually. The examination revealed the presence of four hypoplasias with a right side dominance, illustrated in Figure 6.2. Notice how the right-hand vessels display a clear increase in diameter when compared to the left side. In contrast, only one hypoplasia with the left side dominant was observed. This discrepancy in the number of hypoplasias between the two sides may provide a plausible explanation for the variations in venous velocities. It is important to highlight that this justification is supported by the mean values of the cross-sectional area, since the right side presents a larger value compared to the left side.

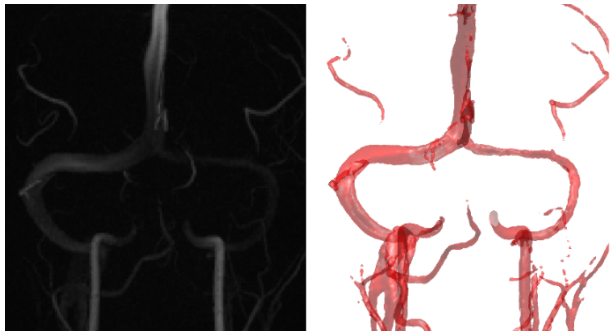

Figure 6.2: Hypoplasia with a dominant right side. **Left**: Sagittal Maximum Intensity Projection, calculated using angiographic image. **Right**: Three-dimensional reconstruction

6.2.3 Cross-sectional Area

Intracranial artery diameters for young, healthy people (aged 18 to 35 years) were measured in two studies [74, 75]. The cross-sectional areas of ICA, MCA and BA, assuming a circular shap, were 15.2 mm^2 to 21.6 mm^2, 6.6 mm^2 to 9.6 mm^2, and 8.04 mm^2 to 9.6 mm^2, respectively. Analysing 5.2, it is possible to conclude that the values obtained in this work are similar to the ones reported in these studies.

Regarding the brain sinuses, a study [76] measured its cross-sectional area before and after a lumbar puncture, and reported results of 40 mm^2 to 52 mm^2 for TS and 52 mm^2 to 54 mm^2 for SSS, which are in accordance with the values showed in this research, as summarized in 5.7

Concerning the cross-sectional area of the arteries and sinuses, the obtained values were found to be consistent with those reported in the existing literature. However, it is important to note that this parameter is considered to be the least reliable among all measured variables. It was suggested that the poor reproducibility of the area measurements can be attributed to the presence of noise that affects the segmentation process. This noise introduces random errors, which, fortunately, do not significantly impact the overall results of the measurements. Despite this limitation, the obtained values still provide valuable insights into the characteristics of the vessels under investigation.

Regarding the venous sinuses, the measured values fell within the reported interval, indicating consistency with previous findings. Notably, a distinction between the left and right sides was observed, as discussed in the preceding subsection. It is important to note that hypoplasia of TS is a frequently encountered anatomical variation. Furthermore, it is worth mentioning that in 61% of all cases, the right TS was found to be dominant [77], what is in line with the findings of this study.

6.2.4 Arterial and Venous Pulsatility Index

Before starting the discussion of the remaining parameters, it is important to acknowledge that these specific parameters have been derived from the calculations based on the aforementioned measurements. It is also important to emphasize that the accuracy and

reliability of these parameters heavily rely on the precision of the measurements conducted. Hence, the analysis of error propagation will be thoroughly examined in the subsequent paragraphs.

The results obtained in the current study, as presented in Table 5.9, were compared to those of several previous studies [38, 40, 78] that have reported PIs ranging from 0.8 to 1, in healthy individuals aged 50 to 91. Additionally, [36] focused on young and healthy individuals, aged 20 to 30, presenting values of 0.71±0.12, for BA; 0.72±0.11, for MCA; and 0.84±0.13, for ICA. Upon comparison, it was observed that the results obtained in this study slightly underestimated the PI values demonstrated in the aforementioned studies, although higher than the values reported by Duarte [13]. However, these values were consistent with the expected trend, as ICA exhibited higher pulsatility (0.62) compared to MCA (0.6) and BA (0.56).

The most significant disparity arises when comparing the values obtained in this work with those assessing the PI for a cohort older than the one included in this study. This notable distinction is to be expected, as research has consistently shown that PI tends to increase with age[10].

Notably, ICA showed the greatest deviation from the literature results, which could be attributed to the specific segment used for calculating the PI. In the study conducted by Zarrinkoob et al. [36] (younger cohort), the measurement sites were described for BA and MCA, but no such information was provided for ICA. It is well-known that pulsatility decreases with increasing vascular distance [10], and this discrepancy from the literature may be due to variations in measurement locations along ICA.

Regarding Venous pulsatility, literature provides some reference values for PIs in the TS and SSS. For instance, Rivera et al. [40] reported PIs going from 0.3 to 0.9. Another study [79] observed values for PI ranged from 0.29 to 0.33, in the venous sinuses in healthy individuals. These findings suggest that the PIs obtained in this study, for venous pulsatility, are aligned with the existing literature.

This is in line with our expectations, as both venous velocities and sinuses' cross-sectional areas were found to be consistent with findings from previous studies. Similar to the velocity, the analysis of PI also uncovered disparities between the left and right sides of the TS, and the same reason can be attributed to this observation.

6.2.5 Flow Volume Pulsatility

In the study conducted by Waahlin et al. [80], FVP values reported were 0.20 ± 0.08 *ml*, for the BA; 0.35 ± 0.10 *ml*, for the ICA; and 0.23 ± 0.05 *ml*, for MCA. However, upon analyzing the data presented in table 5.9, it can be observed that FVP values obtained in this particular study are slightly higher than those reported by Waahlin et al. [80].

This discrepancy can potentially be attributed to the methodology employed in calculating FVP, which relies on the measurement of blood flow. It is worth noting that the

blood flow values used in the calculation are derived from velocity measurements, which we have previously identified as being overestimated.

6.2.6 Wall Shear Stress

In a study of 301 healthy volunteers [74], the WSS was measured in major cerebral arteries, and reported values of $2.2 \pm 0.6\ Pa$, $2.3 \pm 0.6\ Pa$, $1.1 \pm 0.3\ Pa$, $1.1 \pm 0.3\ Pa$ and $1.9 \pm 0.6\ Pa$ for left and right MCA, left and right ICA and BA, respectively. According to a review article [81], the normal values for WSS were defined as 1.0 *Pa* for large arteries and 1.6 *Pa* for small arteries.

Upon revisiting table 5.9, it can be seen that values for ICA are slightly higher, whereas the values of WSS for MCA and BA are consistent with the findings reported in the literature.

To calculate WSS, the first step involved determining the peak velocities across the cross-sectional area of the vessel of the entire cardiac cycle. All these peak velocities were then averaged over the cardiac cycle. This means that all peak velocities, including both the maximum and minimum peak velocity values, were used in the calculation of WSS.

The peak velocity of the ICA was found to be underestimated, and the reason attributed was the specific segment used for the analysis. However, despite this underestimation, the WSS values for the ICA were overestimated. As discussed in section **??**, the maximum velocity at the end of the diastole was consistently overestimated, which could have led to an overall overestimation of the WSS. Yet, it is worth mentioning that the difference in the overestimation was minimal.

Based on the discussions so far, it can be concluded that the increased VENC played a significant role in the overestimation of the ICA's WSS.

6.2.7 Pulse Wave Velocity

No previous investigations were found for PWV of the intracranial segment of ICA. However, in a previous research paper [82], PWV between ICA and common carotid artery was measured in a group of young healthy volunteers, and the value found was $4.7 \pm 1.0\ m/s$.

Another study [34], measured PWV between the cervical segment and the petrous segment of ICA in healthy, but elderly individuals and found it to range from 4.1 *m/s* to 10 *m/s*, using two different reconstruction techniques.

A more recent study [35] assessed cerebral arterial PWV in the intracranial vascular tree, and presented a value of 10.7 *m/s* for a young cohort.

In the present study, PWV across the internal segment of the right and left ICA was measured and the values obtained were $5.2 \pm 2.6\ m/s$ and $4.8 \pm 2.4\ m/s$, respectively. Those are within an acceptable agreement with [34], but slightly underestimated when compared to [35].

By analyzing the papers mentioned in the previous paragraphs, we can attempt to understand the values obtained in this study. Firstly, it is important to acknowledge that the segment analyzed in this study differs from those examined in the other studies found. This distinction is significant because potential differences in arterial compliance between measurement segments can impact the measurements of the PWV.

Both [34, 35] reported high PWV values in different segments, and these findings can be explained as follows. In the study by Bjornfot et al. [35], PWV was calculated in the whole intracranial vascular tree, which increased the distance between the two measurement sites, resulting in higher PWV values.

In the second study by Rivera et al. [34], the values obtained fell within the lower limit of the interval. However, this can be attributed to the fact that an elderly cohort was examined in that study. It is well-documented in the literature that age has an impact on PWV, and it is expected that PWV values would be lower in younger individuals [83, 84].

6.2.8 Pressure Drop

As mentioned in chapter 4, the calculation of PD followed a method commonly used to determine pressure drops, in cases of stenosis. However, since this study focused on a cohort of healthy individuals, no stenosis was expected or observed. Nevertheless, this parameter was utilized to calculate pressure drops within the same vessel or at bifurcations.

It was anticipated that the PD values would be close to zero, since we are analyzing healthy vessels. In a study conducted by Vali et al. [85], pressure drops were calculated for moderate and severe stenosis, yielding values ranging from 2 $mmHg$ to 3.5 $mmHg$.

In our study, when measuring PD within the same healthy vessels, we observed values ranging from 0.3 $mmHg$ to 0.4 $mmHg$. These drops could be attributed to the fact that measurements were taken at distant sites within the same vessel. On the other hand, when assessing PD at bifurcations, higher values were observed (0.63 $mmHg$ and 0.76 $mmHg$), as expected, due to variations in velocity and cross-sectional area estimates. As could be expected, all PD values were significantly different from the ones measured at stenoses.

Although these values appear reasonable and this parameter can be useful for stenosis evaluation, it is important to note that there are more effective methods for assessing PD in healthy vessels, such as using pressure maps, based on the Navier-Stokes equation.

6.2.9 Total blood inflow and outflow

In a study conducted by Shi et al. [79], the total cerebral arterial flow was reported to be $776.90 \pm 125.33\ mL/min$, while the mean IJV flow was $597.47 \pm 195.05\ mL/min$. These values contrast with the substantially lower values found in the present study for both arterial inflow and venous outflow.

The differences between the results found in this research and those reported in the literature can be attributed to various factors. For instance, in Shi et al.'s study [79], the

total arterial flow was calculated by considering the flow from both ICA and the vertebral arteries. In contrast, the present study focused on the ICA and BA, which may have led to an underestimation of the total arterial flow.

Regarding the venous outflow, the lower values observed in this study could be attributed to the specific segment used for the calculation. In this study, the Sigmoid Sinus was utilized, whereas Shi et al.'s study [79] employed the IJV. It is important to note that the inferior petrosal sinuses join the sigmoid sinus to form the IJV. Therefore, it is understandable that the sigmoid sinus would exhibit lower flow compared to the IJV.

7

Conclusion

To finish this thesis, a presentation of the main conclusions of the project and the identification of its limitations will be provided. Additionally, suggestions to overcome these limitations and future perspectives for research will be discussed to conclude the chapter.

7.1 Summary of findings

To assess the suitability of the chosen VENC for this research, a reproducibility analysis was conducted. Contrary to the findings of Duarte's research [13], the cross-sectional area of the vessels exhibited the poorest results. Specifically, BA and right MCA showed poor results, which may be attributed to noise present in the images, which affects the segmentation of the cross-sectional area.

Furthermore, both BA and right MCA demonstrated poor results for peak velocity. This can be explained by the fact that peak velocity is more susceptible to noise interference. However, when considering other parameters such as maximum, minimum, and mean velocities, across all vessels, moderate to very good results were observed. This suggests that averaging the velocities along the cross-sectional segment can help mitigate the influence of peak noise.

Although the reliability of the measurements was not as high as expected, it was still not significantly poor. This finding is supported by the results of the Paired t-Test, which indicated no significant difference between the paired observations of the variable taken on the two days. This suggests that the noise did not have a substantial impact on the measurements. It is important to consider that the relatively small cohort size may have contributed to the observed differences affecting reproducibility.

When examining each vessel individually, the right MCA and BA showed the poorest results. The poor results in BA can be attributed to the presence of an identified outlier, while the right MCA's tortuous and small nature makes it challenging to obtain accurate measurements.

Overall, while the reproducibility of the measurements was not optimal, the results of the Paired t-Test test provide reassurance that the observed differences were not statistically

significant.

The comparison with other studies revealed contrasting findings to those of Duarte's research [13]. Specifically, it was observed that some arterial velocities were overestimated. One possible explanation is that peak noise may have led to the overestimation of true peak velocities. Additionally, it was noted that the choice of the segment used to measure velocities can interfere with the accuracy of the measurements, as velocities can vary within different segments of the vessel.

This overestimation of velocities subsequently resulted in an overestimation of WSS and FVP, as these parameters rely on accurate velocity estimates for their calculations. The propagation of errors in velocity estimation can have significant implications for the interpretation of these parameters.

Although there were no reported values for PD and PWV in the literature for comparison, the discussion led to the conclusion that the calculated values were within a reasonable range. Regarding the PI, it was found that the values were still underestimated. However, the values obtained in this study were higher than those reported by Duarte [13].

Furthermore, it was observed that the total blood inflow and outflow values were underestimated. As discussed, this underestimation could be attributed to the specific vessels or sinuses chosen for the calculations, as well as potential limitations in the measurement techniques employed.

About the venous study, all the results, namely velocity and PI, were within the reported interval, indicating that the chosen VENC was appropriate for the analysis. This finding suggests that the selected VENC value effectively captured the range of velocities and pulsatility in the venous system under investigation.

7.2 Identified Limitations and Proposed Solutions

Several limitations were observed in this study, which resulted in suboptimal reproducibility and differences compared to the existing literature. In the following paragraphs, I will summarize those limitations and provide suggestions to overcome them.

One limitation of this study was the high VENC used, which led to high levels of noise. Throughout this thesis, the impact of noise on the results has been discussed. To address this issue, several suggestions can be considered:

- To Decrease the VENC: Choose a value for the VENC less than 150 *cm/s*, with the caution that this should be set to a value higher than 80 cm/s (as Daurte reported aliasing with this value).
- To avoid the high levels of noise: Apply denoising techniques such as Gaussian filtering, median filtering, or wavelet denoising to reduce the noise in the image.
- To improve vessel's segmentation: Implement post-processing techniques like morphological operations (e.g., erosion, dilation) or region-growing algorithms to refine the segmentation result and remove any remaining noise artefacts.

- To improve vessel's segmentation: Explore the use of machine learning algorithms, such as convolutional neural networks, for vessel segmentation. These algorithms can learn to differentiate between vessel structures and noise, leading to more accurate segmentations [86].
- To improve signal-to-noise ratio: Optimize certain sequence parameters such as section thickness, flip angle, echo time, and receiver bandwidth. However, it is important to consider that increasing the echo time can make the sequence more susceptible to motion artefacts, and increasing the section thickness may result in significant partial volume effects in smaller blood vessels [87].

Another limitation is the small cohort of participants. Since the study population is limited, outliers and minor differences can have a significant impact on the results. For future work, it is recommended to use a larger cohort to improve the reliability and statistical power of the findings.

The nonisotropic and reduced spatial resolutions of the collected images, when compared to other studies, may also be a limiting factor. Increasing the spatial resolution could be an interesting approach to address this limitation.

Another limitation of this study that may have contributed to the not so satisfactory results of the reproducibility study was the time gap between the measurements. It is recommended to avoid a six-week time difference, as numerous physiological events can occur during this period, and environmental factors such as weather can influence the brain's hemodynamics.

Furthermore, comparing the results of this study with the literature was challenging due to the influence of age and health on the calculated parameters. Additionally, the choice of vessel segment highly affects measurements. To overcome these obstacles, it is suggested to extend the cohort to include a wider range of ages and to extract measurements from multiple segments of the same vessel.

Another limitation found in this methodology is the consistent underestimation of the PI, as observed in this research and Duarte [13]. To obtain a more reliable value for PI, it is suggested to change the way flows are calculated, since they are required for PI's calculation (see equation 4.1). Instead of multiplying the velocity by a fixed value of the vessel's cross-sectional area, it is recommended to account for vessel compliance. For example, adjusting the threshold used for segmentation based on the cardiac phase can help calculate a more reliable PI.

7.3 Future Perspectives

As this thesis integrates a project aimed at evaluating and characterizing CSVD, there are still future tasks that need to be addressed in order to achieve this goal. These tasks will contribute to a better understanding of CSVD and its implications.

Since the venous study yielded positive results when compared with existing literature, it would be beneficial to assess the reproducibility of this study. Understanding the

pulsatility of the venous system can provide valuable insights for the assessment of various brain diseases, conducting further investigations to validate the findings of this study would be of great interest.

The initial objective of this thesis was to extract 4D flow data from healthy subjects before and after intense physical exercise. By incorporating physical exercise into the evaluation process, we can gain a better understanding of how the methodology performs under varying conditions. Therefore, in order to advance this research, it is important to evaluate the methodology in different physiological environments.

Furthermore, it is crucial to expand the collection of data from both patients suffering from CSVD and healthy individuals within the same age range. By combining this data with that of young and healthy individuals, a comparative study can be conducted to gain further insights. This comparative analysis will provide a comprehensive understanding of the differences and similarities between CSVD patients and healthy individuals.

7.4 Study Contribution

Firstly, in this work, additional features were incorporated into an existing post-processing tool [61]. These new features include the calculation of several parameters that aid in understanding the hemodynamics of blood in the intracranial vessels and sinuses. By adding these calculations, a more comprehensive analysis of the blood flow characteristics could be achieved.

The comprehensive study of the parameters has resulted in a deeper understanding of their relation with velocity measurements. Through meticulous analysis of those parameters, their interplay and impact on the overall hemodynamics have been elucidated, thereby making a significant contribution to the advancement of knowledge in this field.

By assessing the effectiveness of the specific VENC values, this thesis represents a step towards the main objective of the project.

Additionally, the results presented in this thesis have also contributed to the normative basis for healthy and young volunteers. By studying these individuals, a baseline understanding of normal hemodynamics can be established, which serves as a reference for future studies involving patients with CSVD

Bibliography

[1] J. M. Lourenço, *The NOVAthesis LaTeX Template User's Manual*, NOVA University Lisbon, 2021. [Online]. Available: https://github.com/joaomlourenco/novathesis/raw/main/template.pdf (cit. on p. ii).

[2] R. J. Cannistraro, M. Badi, B. H. Eidelman, D. W. Dickson, E. H. Middlebrooks, and J. F. Meschia, "Cns small vessel disease: A clinical review", *Neurology*, vol. 92, pp. 1146–1156, 24 2019-06, ISSN: 1526632X. DOI: 10.1212/WNL.0000000000007654 (cit. on p. 1).

[3] P. Brodal, *The Central Nervous System*, 4th. Oxford University Press, 2010, ISBN: 9780190251499. (Cit. on p. 1).

[4] J. M. Wardlaw, C. Smith, and M. Dichgans, "Mechanisms of sporadic cerebral small vessel disease: Insights from neuroimaging", *The Lancet Neurology*, vol. 12, no. 5, pp. 483–497, 2013 (cit. on p. 1).

[5] B. Ren *et al.*, "Cerebral small vessel disease: Neuroimaging features, biochemical markers, influencing factors, pathological mechanism and treatment", *Frontiers in Neurology*, vol. 13, p. 1157, 2022-06, ISSN: 16642295. DOI: 10.3389/FNEUR.2022.843953/BIBTEX (cit. on p. 1).

[6] G. W. Blair, M. V. Hernandez, M. J. Thrippleton, F. N. Doubal, and J. M. Wardlaw, "Advanced neuroimaging of cerebral small vessel disease", *Current Treatment Options in Cardiovascular Medicine*, vol. 19, p. 56, 7 2017-07, ISSN: 1092-8464. DOI: 10.1007/s11936-017-0555-1. [Online]. Available: http://link.springer.com/10.1007/s11936-017-0555-1 (cit. on pp. 1, 6).

[7] J. M. Wardlaw, C. Smith, and M. Dichgans, "Small vessel disease: Mechanisms and clinical implications", *The Lancet Neurology*, vol. 18, pp. 684–696, 7 2019-07, ISSN: 14744465. DOI: 10.1016/S1474-4422(19)30079-1 (cit. on p. 1).

[8] J.-C. Ferré, E. Bannier, H. Raoult, G. Mineur, B. Carsin-Nicol, and J.-Y. Gauvrit, "Arterial spin labeling (asl) perfusion: Techniques and clinical use", *Diagnostic and Interventional Imaging*, vol. 94, pp. 1211–1223, 12 2013-12, ISSN: 22115684. DOI:

10.1016/j.diii.2013.06.010. [Online]. Available: https://linkinghub.elsevier.com/retrieve/pii/S221156841300209X (cit. on p. 2).

[9] S. Meckel *et al.*, "Intracranial artery velocity measurement using 4d pc mri at 3 t: Comparison with transcranial ultrasound techniques and 2d pc mri", *Neuroradiology*, vol. 55, pp. 389–398, 2013 (cit. on pp. 2, 9, 30, 31).

[10] A. Wåhlin, A. Eklund, and J. Malm, "4d flow mri hemodynamic biomarkers for cerebrovascular diseases", *Journal of Internal Medicine*, vol. 291, no. 2, pp. 115–127, 2022 (cit. on pp. 2, 6, 7, 15, 16, 33).

[11] J. F. Juffermans *et al.*, "Reproducibility of aorta segmentation on 4d flow mri in healthy volunteers", *Journal of Magnetic Resonance Imaging*, vol. 53, no. 4, pp. 1268–1279, 2021 (cit. on p. 2).

[12] M. Markl, A. Frydrychowicz, S. Kozerke, M. Hope, and O. Wieben, "4d flow mri", *Journal of Magnetic Resonance Imaging*, vol. 36, pp. 1015–1036, 5 2012-11, ISSN: 10531807. DOI: 10.1002/jmri.23632. [Online]. Available: https://onlinelibrary.wiley.com/doi/10.1002/jmri.23632 (cit. on pp. 2, 8).

[13] A. M. Duarte, "A reproducibility study of 4d flow mri in intracranial vessels", 2022 (cit. on pp. 2, 9, 13, 15, 27, 33, 37–39).

[14] T. T. LIU and G. G. BROWN, "Measurement of cerebral perfusion with arterial spin labeling: Part 1. methods", *Journal of the International Neuropsychological Society*, vol. 13, pp. 517–525, 03 2007-05, ISSN: 1355-6177. DOI: 10.1017/S1355617707070646. [Online]. Available: http://www.journals.cambridge.org/abstract_S1355617707070646 (cit. on p. 4).

[15] J. Valenta, L. Páč, J. Stignl, and P. Fiala, *Central Nervous System : Overview of Anatomy*, 1st. Karolium Press, 2012, ISBN: 9788024626475. (Cit. on p. 4).

[16] J. V. Campellone, *Circle of willis: Medlineplus medical encyclopedia image*, 2023-04. [Online]. Available: https://medlineplus.gov/ency/imagepages/18009.htm (cit. on p. 5).

[17] W. F. Boron and E. L. Boulpaep, *Medical physiology E-book*. Elsevier Health Sciences, 2016 (cit. on p. 5).

[18] T. Kılıç and A. Akakın, "Anatomy of cerebral veins and sinuses", *Handbook on cerebral venous thrombosis*, vol. 23, pp. 4–15, 2008 (cit. on p. 5).

[19] A. O. Safadi and P. Tadi, "Anatomy, head and neck, cerebral venous system", 2020 (cit. on p. 5).

[20] M. A. Uddin, T. U. Haq, and M. Z. Rafique, "Cerebral venous system anatomy", *Journal of Pakistan Medical Association*, vol. 56, no. 11, p. 516, 2006 (cit. on p. 5).

[21] S. Kunhumon, "Cerebral vein thrombosis misdiagnosed and mismanaged", *Thrombosis*, vol. 2012, p. 210 676, 2012-04. DOI: 10.1155/2012/210676 (cit. on p. 5).

[22] B. V. Zlokovic, "The blood-brain barrier in health and chronic neurodegenerative disorders", *Neuron*, vol. 57, pp. 178–201, 2 2008-01, ISSN: 08966273. DOI: 10.1016/j.neuron.2008.01.003. [Online]. Available: https://linkinghub.elsevier.com/retrieve/pii/S0896627308000342 (cit. on p. 5).

[23] M. F. O'Rourke and J. Hashimoto, "Mechanical factors in arterial aging: A clinical perspective", *Journal of the American College of Cardiology*, vol. 50, no. 1, pp. 1–13, 2007, ISSN: 0735-1097. DOI: https://doi.org/10.1016/j.jacc.2006.12.050. [Online]. Available: https://www.sciencedirect.com/science/article/pii/S0735109707012636 (cit. on p. 6).

[24] G. M. London and B. Pannier, "Arterial functions: how to interpret the complex physiology", *Nephrology Dialysis Transplantation*, vol. 25, no. 12, pp. 3815–3823, 2010-10, ISSN: 0931-0509. DOI: 10.1093/ndt/gfq614. eprint: https://academic.oup.com/ndt/article-pdf/25/12/3815/5284078/gfq614.pdf. [Online]. Available: https://doi.org/10.1093/ndt/gfq614 (cit. on p. 6).

[25] Q. Li *et al.*, "Cerebral small vessel disease", *Cell Transplantation*, vol. 27, pp. 1711–1722, 12 2018-12, ISSN: 0963-6897. DOI: 10.1177/0963689718795148. [Online]. Available: http://journals.sagepub.com/doi/10.1177/0963689718795148 (cit. on p. 6).

[26] L. Pantoni, "Cerebral small vessel disease: From pathogenesis and clinical characteristics to therapeutic challenges", *The Lancet Neurology*, vol. 9, pp. 689–701, 7 2010-07, ISSN: 14744422. DOI: 10.1016/S1474-4422(10)70104-6. [Online]. Available: https://linkinghub.elsevier.com/retrieve/pii/S1474442210701046 (cit. on p. 6).

[27] G. W. Blair *et al.*, "Intracranial hemodynamic relationships in patients with cerebral small vessel disease", *Neurology*, vol. 94, e2258–e2269, 21 2020-05, ISSN: 0028-3878. DOI: 10.1212/WNL.0000000000009483. [Online]. Available: https://n.neurology.org/content/94/21/e2258%20https://n.neurology.org/content/94/21/e2258.abstract (cit. on p. 6).

[28] U. Khan, L. Porteous, A. Hassan, and H. S. Markus, "Risk factor profile of cerebral small vessel disease and its subtypes", *Journal of Neurology, Neurosurgery Psychiatry*, vol. 78, pp. 702–706, 7 2006-12, ISSN: 0022-3050. DOI: 10.1136/jnnp.2006.103549. [Online]. Available: https://jnnp.bmj.com/lookup/doi/10.1136/jnnp.2006.103549 (cit. on p. 6).

[29] M. F. O'Rourke and M. E. Safar, "Relationship between aortic stiffening and microvascular disease in brain and kidney", *Hypertension*, vol. 46, pp. 200–204, 1 2005-07, ISSN: 0194-911X. DOI: 10.1161/01.HYP.0000168052.00426.65. [Online]. Available: https://www.ahajournals.org/doi/10.1161/01.HYP.0000168052.00426.65 (cit. on p. 6).

[30] A. Mahammedi *et al.*, "Small vessel disease, a marker of brain health: What the radiologist needs to know", *American Journal of Neuroradiology*, vol. 43, pp. 650–660, 5 2022-05, ISSN: 0195-6108. DOI: 10.3174/AJNR.A7302. [Online]. Available: http://www.ajnr.org/content/43/5/650%20http://www.ajnr.org/content/43/5/650.abstract (cit. on p. 6).

[31] M. Pasi and C. Cordonnier, "Clinical relevance of cerebral small vessel diseases", *Stroke*, vol. 51, pp. 47–53, 1 2020-01, ISSN: 15244628. DOI: 10.1161/STROKEAHA.119.024148. [Online]. Available: https://www.ahajournals.org/doi/abs/10.1161/STROKEAHA.119.024148 (cit. on p. 6).

[32] Z. Cai *et al.*, "Cerebral small vessel disease and alzheimer disease", *Clinical Interventions in Aging*, vol. 10, p. 1695, 2015-10, ISSN: 1178-1998. DOI: 10.2147/CIA.S90871. [Online]. Available: https://www.dovepress.com/cerebral-small-vessel-disease-and-alzheimerrsquos-disease-peer-reviewed-article-CIA (cit. on p. 6).

[33] C. Guy and D. Ffytche, *The Principles of Medical Imaging*, Revised Edition. Imperial College Press, 2005, ISBN: 1-86094-502-3 (cit. on pp. 6, 7).

[34] L. A. Rivera-Rivera *et al.*, "Assessment of vascular stiffness in the internal carotid artery proximal to the carotid canal in alzheimer's disease using pulse wave velocity from low rank reconstructed 4d flow mri", *Journal of Cerebral Blood Flow & Metabolism*, vol. 41, no. 2, pp. 298–311, 2021 (cit. on pp. 6, 34, 35).

[35] C. Björnfot, A. Garpebring, S. Qvarlander, J. Malm, A. Eklund, and A. Wåhlin, "Assessing cerebral arterial pulse wave velocity using 4d flow mri", *Journal of Cerebral Blood Flow & Metabolism*, vol. 41, no. 10, pp. 2769–2777, 2021 (cit. on pp. 6, 34, 35).

[36] L. Zarrinkoob *et al.*, "Aging alters the dampening of pulsatile blood flow in cerebral arteries", *Journal of Cerebral Blood Flow & Metabolism*, vol. 36, no. 9, pp. 1519–1527, 2016 (cit. on pp. 7, 33).

[37] V. Mehta and E. Tzima, "A turbulent path to plaque formation", *Nature*, vol. 540, no. 7634, pp. 531–532, 2016 (cit. on p. 7).

[38] T. Vikner, L. Nyberg, M. Holmgren, J. Malm, A. Eklund, and A. Wåhlin, "Characterizing pulsatility in distal cerebral arteries using 4d flow mri", *Journal of Cerebral Blood Flow & Metabolism*, vol. 40, no. 12, pp. 2429–2440, 2020 (cit. on pp. 7, 33).

[39] F. Garcia-Polite *et al.*, "Pulsatility and high shear stress deteriorate barrier phenotype in brain microvascular endothelium", *Journal of Cerebral Blood Flow & Metabolism*, vol. 37, no. 7, pp. 2614–2625, 2017 (cit. on p. 7).

[40] L. A. Rivera-Rivera *et al.*, "Changes in intracranial venous blood flow and pulsatility in alzheimer's disease: A 4d flow mri study", *Journal of Cerebral Blood Flow & Metabolism*, vol. 37, no. 6, pp. 2149–2158, 2017 (cit. on pp. 7, 33).

[41] S. E. Berman *et al.*, "Intracranial arterial 4d flow in individuals with mild cognitive impairment is associated with cognitive performance and amyloid positivity", *Journal of Alzheimer's Disease*, vol. 60, no. 1, pp. 243–252, 2017 (cit. on p. 7).

[42] D. W. McRobbie, E. A. Moore, M. J. Graves, and M. R. Prince, *MRI From Picture to Proton*. 2004 (cit. on pp. 7, 8).

[43] D. Thomas and J. Wells, *Mr angiography and arterial spin labelling*, 2011. DOI: 10.1007/978-1-61737-992-5_16 (cit. on p. 7).

[44] J. Suresh, P. Subha, and G. Raveendran, *Understanding Phase Contrast MR Angiography A Practical Approach with MATLAB Examples*. 2016. [Online]. Available: http://www.springer.com/series/10059 (cit. on p. 7).

[45] S. W. Youn and J. Lee, "From 2d to 4d phase-contrast mri in the neurovascular system: Will it be a quantum jump or a fancy decoration?", *Journal of Magnetic Resonance Imaging*, vol. 55, pp. 347–372, 2 2022-02, ISSN: 1053-1807. DOI: 10.1002/jmri.27430. [Online]. Available: https://onlinelibrary.wiley.com/doi/10.1002/jmri.27430 (cit. on pp. 7, 8).

[46] J. Ramalho and M. Castillo, "Vascular imaging of the central nervous system: Physical principles, clinical applications, and emerging techniques", 2014 (cit. on pp. 7, 8).

[47] P. Vilela, "Phase contrast magnetic resonance angiography (pc mra) and flow analysis: Clinical applications", *Vascular imaging of the central nervous system: Physical principles, clinical applications, and emerging techniques*, pp. 161–175, 2014 (cit. on p. 8).

[48] L. Wigström, L. Sjöqvist, and B. Wranne, "Temporally resolved 3d phase-contrast imaging", *Magnetic resonance in medicine*, vol. 36, no. 5, pp. 800–803, 1996 (cit. on p. 8).

[49] G. Soulat, P. McCarthy, and M. Markl, "4d flow with mri", *Annual Review of Biomedical Engineering*, vol. 22, pp. 103–126, 1 2020-06, ISSN: 1523-9829. DOI: 10.1146/annurev-bioeng-100219-110055. [Online]. Available: https://www.annualreviews.org/doi/10.1146/annurev-bioeng-100219-110055 (cit. on p. 8).

[50] R. Aaslid, *Transcranial doppler sonography*. Springer Science & Business Media, 2012 (cit. on p. 9).

[51] S.-Y. Ha, Y. Kang, H.-J. Lee, M. Hwang, J. Baik, and S. Park, "Intracranial flow velocity quantification using non-contrast four-dimensional flow mri: A prospective comparative study with transcranial doppler ultrasound", *Diagnostics*, vol. 12, p. 23, 1 2021-12, ISSN: 2075-4418. DOI: 10.3390/diagnostics12010023. [Online]. Available: https://www.mdpi.com/2075-4418/12/1/23 (cit. on pp. 9, 30).

[52] A. G. Morgan, M. J. Thrippleton, J. M. Wardlaw, and I. Marshall, "4d flow mri for non-invasive measurement of blood flow in the brain: A systematic review", *Journal of Cerebral Blood Flow Metabolism*, vol. 41, pp. 206–218, 2 2021-02, ISSN: 0271-678X. DOI: 10.1177/0271678X20952014. [Online]. Available: http://journals.sagepub.com/doi/10.1177/0271678X20952014 (cit. on p. 9).

[53] Y. Shi, M. J. Thrippleton, I. Marshall, and J. M. Wardlaw, "Intracranial pulsatility in patients with cerebral small vessel disease: A systematic review", *Clinical Science*, vol. 132, pp. 157–171, 1 2018-01, ISSN: 0143-5221. DOI: 10.1042/CS20171280. [Online]. Available: https://portlandpress.com/clinsci/article/132/1/157/71669/Intracranial-pulsatility-in-patients-with-cerebral (cit. on p. 10).

[54] C. R. Stewart, M. S. Stringer, Y. Shi, M. J. Thrippleton, and J. M. Wardlaw, "Associations between white matter hyperintensity burden, cerebral blood flow and transit time in small vessel disease: An updated meta-analysis", *Frontiers in Neurology*, vol. 12, p. 621, 2021-05, ISSN: 16642295. DOI: 10.3389/FNEUR.2021.647848/BIBTEX (cit. on p. 10).

[55] Y. Shi *et al.*, "Cerebral blood flow in small vessel disease: A systematic review and meta-analysis", *Journal of Cerebral Blood Flow Metabolism*, vol. 36, pp. 1653–1667, 10 2016-10, ISSN: 0271-678X. DOI: 10.1177/0271678X16662891. [Online]. Available: http://journals.sagepub.com/doi/10.1177/0271678X16662891 (cit. on p. 10).

[56] K.-W. Nam, H.-M. Kwon, and Y.-S. Lee, "Distinct association between cerebral arterial pulsatility and subtypes of cerebral small vessel disease", *PLOS ONE*, vol. 15, M. Mogi, Ed., e0236049, 7 2020-07, ISSN: 1932-6203. DOI: 10.1371/journal.pone.0236049. [Online]. Available: https://dx.plos.org/10.1371/journal.pone.0236049 (cit. on p. 10).

[57] W. Lu, C. Yu, L. Wang, F. Wang, and J. Qiu, "Perfusion heterogeneity of cerebral small vessel disease revealed via arterial spin labeling mri and machine learning", *NeuroImage: Clinical*, vol. 36, p. 103 165, 2022-01, ISSN: 2213-1582. DOI: 10.1016/J.NICL.2022.103165 (cit. on p. 10).

[58] J. Birnefeld, A. Wåhlin, A. Eklund, and J. Malm, "Cerebral arterial pulsatility is associated with features of small vessel disease in patients with acute stroke and tia: A 4d flow mri study", *Journal of Neurology*, vol. 267, pp. 721–730, 2020 (cit. on p. 10).

[59] S.-Y. Chuang *et al.*, "Associations of blood pressure and carotid flow velocity with brain volume and cerebral small vessel disease in a community-based population", *Translational stroke research*, vol. 12, pp. 248–258, 2021 (cit. on p. 11).

[60] T. M. Inc., *Matlab version: 9.13.0 (r2022b)*, Natick, Massachusetts, United States, 2022. [Online]. Available: https://www.mathworks.com (cit. on p. 13).

[61] E. Schrauben *et al.*, "Fast 4d flow mri intracranial segmentation and quantification in tortuous arteries", *Journal of Magnetic Resonance Imaging*, vol. 42, pp. 1458–1464, 5 2015-11, ISSN: 10531807. DOI: 10.1002/jmri.24900. [Online]. Available: https://onlinelibrary.wiley.com/doi/10.1002/jmri.24900 (cit. on pp. 13–17, 40).

[62] M. Ziegler, J. Alfraeus, E. Good, J. Engvall, E. De Muinck, and P. Dyverfeldt, "Exploring the relationships between hemodynamic stresses in the carotid arteries", *Frontiers in Cardiovascular Medicine*, vol. 7, p. 617 755, 2021 (cit. on p. 16).

[63] M. Markl *et al.*, "In vivo wall shear stress distribution in the carotid artery: Effect of bifurcation geometry, internal carotid artery stenosis, and recanalization therapy", *Circulation: Cardiovascular Imaging*, vol. 3, no. 6, pp. 647–655, 2010 (cit. on p. 16).

[64] I. Bargiotas *et al.*, "Estimation of aortic pulse wave transit time in cardiovascular magnetic resonance using complex wavelet cross-spectrum analysis", *Journal of Cardiovascular Magnetic Resonance*, vol. 17, pp. 1–11, 2015 (cit. on p. 16).

[65] T. Dunås, A. Wåhlin, L. Zarrinkoob, J. Malm, and A. Eklund, "4d flow mri—automatic assessment of blood flow in cerebral arteries", *Biomedical Physics & Engineering Express*, vol. 5, no. 1, p. 015 003, 2018 (cit. on p. 17).

[66] J. D. Hunter, "Matplotlib: A 2d graphics environment", *Computing in Science & Engineering*, vol. 9, no. 3, pp. 90–95, 2007. DOI: 10.1109/MCSE.2007.55 (cit. on p. 18).

[67] S. Ogoh *et al.*, "The effect of changes in cardiac output on middle cerebral artery mean blood velocity at rest and during exercise", *The Journal of physiology*, vol. 569, no. 2, pp. 697–704, 2005 (cit. on p. 29).

[68] L. Niehaus, S. Gottschalk, and U. Weber, "Effect of drug-induced vasodilatation of basal brain arteries with nitroglycerin on blood flow velocity and volume flow in the middle cerebral artery", *Ultraschall in der Medizin (Stuttgart, Germany: 1980)*, vol. 19, no. 5, pp. 225–229, 1998 (cit. on p. 29).

[69] V. Babikian *et al.*, "Transcranial doppler validation pilot study", *Journal of Neuroimaging*, vol. 3, no. 4, pp. 242–249, 1993 (cit. on p. 30).

[70] B. Wen *et al.*, "Test–retest multisite reproducibility of neurovascular 4d flow mri", *Journal of Magnetic Resonance Imaging*, vol. 49, no. 6, pp. 1543–1552, 2019 (cit. on pp. 30, 31).

[71] R. J. van Tuijl, Y. M. Ruigrok, B. K. Velthuis, I. C. van der Schaaf, G. J. Rinkel, and J. J. Zwanenburg, "Velocity pulsatility and arterial distensibility along the internal carotid artery", *Journal of the American Heart Association*, vol. 9, no. 16, e016883, 2020 (cit. on p. 30).

[72] E. Stolz, M. Kaps, A. Kern, S. S. Babacan, and W. Dorndorf, "Transcranial color-coded duplex sonography of intracranial veins and sinuses in adults: Reference data from 130 volunteers", *Stroke*, vol. 30, no. 5, pp. 1070–1075, 1999 (cit. on p. 31).

[73] R. W. Baumgartner, F. Gönner, M. Arnold, and R. M. Müri, "Transtemporal power- and frequency-based color-coded duplex sonography of cerebral veins and sinuses.", *American journal of neuroradiology*, vol. 18, no. 9, pp. 1771–1781, 1997 (cit. on p. 31).

[74] X. Zhao, M. Zhao, S. Amin-Hanjani, X. Du, S. Ruland, and F. T. Charbel, "Wall shear stress in major cerebral arteries as a function of age and gender—a study of 301 healthy volunteers", *Journal of Neuroimaging*, vol. 25, no. 3, pp. 403–407, 2015 (cit. on pp. 32, 34).

[75] B. G. Fico *et al.*, "The impact of aging on the association between aortic stiffness and cerebral pulsatility index", *Frontiers in cardiovascular medicine*, vol. 9, p. 821 151, 2022 (cit. on p. 32).

[76] S. Lublinsky, A. Friedman, A. Kesler, D. Zur, R. Anconina, and I. Shelef, "Automated cross-sectional measurement method of intracranial dural venous sinuses", *American Journal of Neuroradiology*, vol. 37, no. 3, pp. 468–474, 2016 (cit. on p. 32).

[77] F. Alper, M. Kantarci, S. Dane, K. Gumustekin, O. Onbas, and I. Durur, "Importance of anatomical asymmetries of transverse sinuses: An mr venographic study", *Cerebrovascular Diseases*, vol. 18, no. 3, pp. 236–239, 2004 (cit. on p. 32).

[78] L. A. Rivera-Rivera *et al.*, "4d flow mri for intracranial hemodynamics assessment in alzheimer's disease", *Journal of Cerebral Blood Flow & Metabolism*, vol. 36, no. 10, pp. 1718–1730, 2016 (cit. on p. 33).

[79] Y. Shi *et al.*, "Small vessel disease is associated with altered cerebrovascular pulsatility but not resting cerebral blood flow", *Journal of Cerebral Blood Flow & Metabolism*, vol. 40, no. 1, pp. 85–99, 2020 (cit. on pp. 33, 35, 36).

[80] A. Wåhlin *et al.*, "Measuring pulsatile flow in cerebral arteries using 4d phase-contrast mr imaging", *American Journal of Neuroradiology*, vol. 34, no. 9, pp. 1740–1745, 2013 (cit. on p. 33).

[81] A. Kamiya, R. Bukhari, and T. Togawa, "Adaptive regulation of wall shear stress optimizing vascular tree function", *Bulletin of mathematical biology*, vol. 46, no. 1, pp. 127–137, 1984 (cit. on p. 34).

[82] E. S. Peper *et al.*, "Regional assessment of carotid artery pulse wave velocity using compressed sensing accelerated high temporal resolution 2d cine phase contrast cardiovascular magnetic resonance", *Journal of Cardiovascular Magnetic Resonance*, vol. 20, pp. 1–12, 2018 (cit. on p. 34).

[83] M. F. Elias, M. A. Robbins, M. M. Budge, W. P. Abhayaratna, G. A. Dore, and P. K. Elias, "Arterial pulse wave velocity and cognition with advancing age", *Hypertension*, vol. 53, no. 4, pp. 668–673, 2009 (cit. on p. 35).

[84] W. J. Rogers *et al.*, "Age-associated changes in regional aortic pulse wave velocity", *Journal of the American College of Cardiology*, vol. 38, no. 4, pp. 1123–1129, 2001 (cit. on p. 35).

[85] A. Vali *et al.*, "Semi-automated analysis of 4d flow mri to assess the hemodynamic impact of intracranial atherosclerotic disease", *Magnetic resonance in medicine*, vol. 82, no. 2, pp. 749–762, 2019 (cit. on p. 35).

[86] M. Haft-Javaherian, L. Fang, V. Muse, C. B. Schaffer, N. Nishimura, and M. R. Sabuncu, "Deep convolutional neural networks for segmenting 3d in vivo multiphoton images of vasculature in alzheimer disease mouse models", *PloS one*, vol. 14, no. 3, e0213539, 2019 (cit. on p. 39).

[87] J. Lotz, C. Meier, A. Leppert, and M. Galanski, "Cardiovascular flow measurement with phase-contrast mr imaging: Basic facts and implementation", *Radiographics*, vol. 22, no. 3, pp. 651–671, 2002 (cit. on p. 39).

I

Complementary results

This annex comprises two sections. The first section includes a table presenting the results of the Shapiro-Wilk test. The second section contains Bland-Altman plots for all variables across all vessels.

I.1 Shapiro-Wilk Test

Table I.1: *p*-values for Shapiro-Wilk test across all parameters (minimum, maximum, mean, peak velocities and vessel's cross-sectional area) of all vessels analysed

Vessel	$\mathbf{V_{min}}$		$\mathbf{V_{max}}$		$\mathbf{V_{mean}}$		**Area**		V_{peak}	
	Day 1	*Day 2*	*Day 1*	*Day 2*	*Day 1*	*Day 2*	*Day 1*	*Day 2*	*Day 1*	*Day 2*
BA	0,060	0,849	0,048	0,534	0,025	0,963	0,003	0,015	0,051	0,378
l ICA	0,593	0,657	0,192	0,500	0,585	0,505	0,770	0,398	0,161	0,016
r ICA	0,514	0,997	0,987	0,595	0,914	0,546	0,650	0,943	0,839	0,669
l MCA	0,226	0,708	0,251	0,330	0,149	0,323	0,176	0,709	0,078	0,736
r MCA	0,521	0,541	0,986	0,713	0,994	0,915	0,001	0,221	0,806	0,006

BA = Basilar Artery; **l ICA** = left Internal Carotid Artery; **r ICA** = right Internal Carotid Artery; **l MCA** = left Middle Cerebral Artery; **r MCA** = right Middle Cerebral Artery;

I.2 Bland-Altman Plots

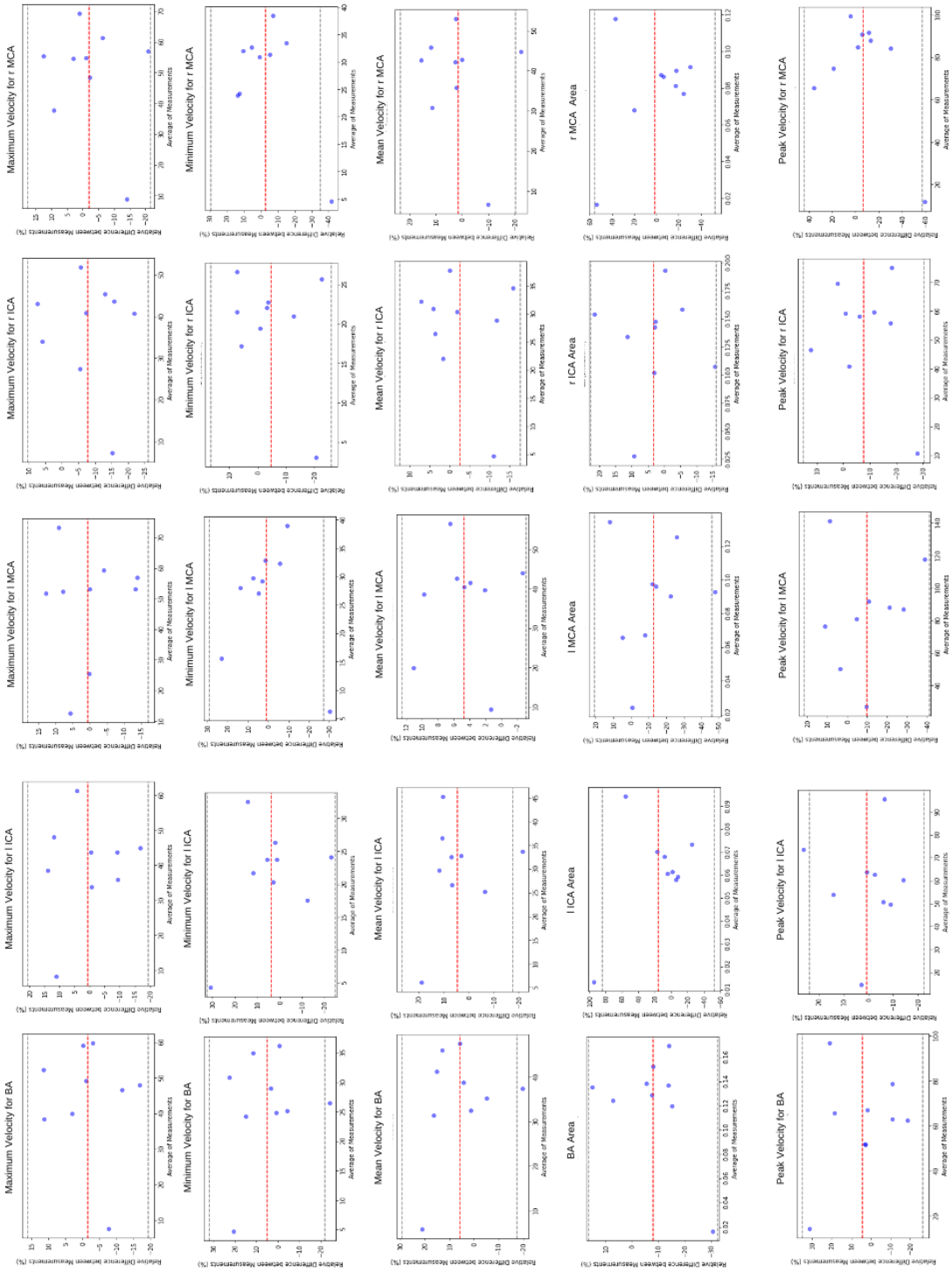

Figure I.1: Bland-Altman plots for every parameter and every vessel assessed